ARCHIVES OF MECHANICS
Arch. Mech. **77** (5), 533–568, 2025, https://doi.org/10.24423/aom.4661

An analytical–numerical approach for the stability analysis of large strain thermo-elastoplastic material models

B. WCISŁO[1*)], J. PAMIN[1)], K. KOWALCZYK-GAJEWSKA[2)], A. MENZEL[3,4)]

[1)] *Chair of Computational Engineering, Cracow University of Technology, Poland, e-mail[*)]: balbina.wcislo@pk.edu.pl (corresponding author)*

[2)] *Institute of Fundamental Technological Research, Polish Academy of Sciences, Poland*

[3)] *Institute of Mechanics, TU Dortmund University, Germany*

[4)] *Division of Solid Mechanics, Lund University, Sweden*

The paper deals with the notion of stability for thermo-elastoplastic materials undergoing large strains. The stability analysis is performed by using the perturbation approach applied to a comprehensive material model derived in a thermodynamic format. As the main contribution of this paper a stability condition for a material model incorporating geometrical and material non-linearities under full thermo-mechanical coupling, without typical simplifying assumptions, is derived, and a hybrid analytical-numerical verification of the stability condition at a material point is investigated for the three-dimensional case. Special emphasis is placed on the quasi-static case, for which a specific stability criterion is derived. The theoretical analysis is followed by the numerical verification of the obtained condition. The implementation of the model in the finite element method, using the numerical-symbolic package AceGen, is also presented in the paper. Two representative three-dimensional examples are solved, namely a cube under simple shear and a plate with imperfection, subjected to tension. The obtained results reveal that the type of softening, i.e., thermal or material softening, has a significant influence on the stability at a material point level.

Key words: material stability, localization, thermo-elastoplasticity, large strains, finite element method.

1. Introduction

In classic mechanics, the notion of stability was related to structural equilibrium. However, already in [1] and [2] the stability of elastic-plastic materials and uniqueness of solutions were discussed. It was then recognized in [3] that an unstable response of a material can lead to the loss of ellipticity of the governing equations (i.e., failure of positive definiteness of the acoustic tensor, associated with the occurrence of a displacement gradient discontinuity) and to

localization of deformation in a small part of a considered specimen (e.g., emerging shear bands). From that moment, the issue of material instabilities and their theoretical and numerical consequences raised considerable interest and produced several approaches to preserve the well-posedness of the considered boundary value problem (BVP), called regularization. It is to be noted that if dynamic conditions (wave propagation) are considered, material instability can lead to the loss of hyperbolicity of the initial boundary value problem (IBVP).

A majority of works were concerned with small inelastic deformations and isothermal conditions. When the numerical simulation of strain localization became one of important issues in computational mechanics, the early considerations on the loss of material stability and well-posedness included [4, 5]. Focusing on the plasticity-related phenomena occurring in metals, finite deformations and rate dependence were taken into account in [6, 7]. The description of shear band formation and evolution was covered in [8]. Ellipticity limits were discussed for instance in [9] for isothermal small strain plasticity. An overview of elastic-plastic instability problems (including buckling and necking localization) was provided in [10]. Special interest was devoted to geomaterials (porous materials) and non-associative plastic flow in, e.g., [11–13].

The issue of regularization of constitutive models and reliable numerical modelling was then the topic of intensive research, see e.g. [14, 15]. Gradient-enhanced continuum models were considered by many researchers, see also [16, 17]. An overview regarding aspects of well-posedness, regularization options and selected applications was provided in [18]. The theories were also built in a finite deformation context, see for instance [19–22]. Books and lecture notes were then written on material instabilities, see [23–26], and the research was further advanced in the book [27]. Instabilities were considered not only in the response of a continuum, but also for interfaces [28].

There are significantly fewer papers on material instabilities when the dependence of the model on temperature is admitted. With the limiting assumption of linear kinematics, the problem is considered for instance in [29–31]. Thermo-inelasticity (in particular plasticity and damage) are discussed in [31] and in some respect it is a starting point of the research presented in this work. Some other contributions on thermo-plasticity focus on so-called adiabatic shear bands, see, e.g., [32–34].

When large strain thermo-elastoplasticity is considered and the models are derived from thermodynamics, several sources can be listed. Thermo-elasticity is investigated in [35–37]. Adiabatic conditions in elastic-plastic materials are considered in [38–40]. Attention is focused on necking in metals in [41].

The analysis of stability is usually performed in one of two ways. The first approach involves the investigation of wave propagation in the material, see, e.g., [31, 33, 42], and is applied in this work. The second method is the analysis

of jump conditions across a discontinuity surface, assuming traction equilibrium at the surface, see, e.g., [21], and, in the case of coupled problems, continuity of the heat flux, see [31].

The aim of the current paper is to derive the conditions for the loss of stability of thermo-elastoplastic material models in the general large deformation format, by using a thermodynamically consistent approach, and to specify such condition for the quasi-static conductive case.

The novel aspect of the paper is thus the derivation of the condition for material stability, which is as general as possible, without simplifications such as small strains, linear material behaviour or internal adiabaticity (understood as the absence of conductivity), which are usually adopted in literature. The derived conditions are original. To the authors' knowledge, large strain conductive thermo-plasticity has not been analysed before in the way presented in the present paper. The advantage of such an approach is that the condition can be applied for a wide range of material models and can answer the question whether the thermo-mechanical coupling provides sufficient regularization. Otherwise, the generated computational results should not be trusted, or an additional regularizing enhancement can be incorporated – for example via an addition of an averaged (non-local) field of a selected quantity, based on the approach proposed in [43] and used in, e.g., [44] or [45], or via the application of a gradient plasticity approach, for instance the one proposed in [46]. However, the main focus of the paper is not to provide a regularization framework (even though sufficient heat conductivity can contribute to the regularization), but to provide an indicator for thermo-plasticity, based, among others, on the acoustic tensor, when material stability is lost at the local level, i.e., at a material point.

Moreover, the results of theoretical derivations are followed by a numerical analysis of the fully coupled thermo-elastoplasticity, which is rarely encountered in literature. For this purpose the thermodynamically consistent material model is implemented within the symbolic-numerical Finite Element Method (FEM) environment AceGen/FEM, and this is performed in a way suitable to take advantage of software capabilities, see [47].

The paper is organized as follows: Section 2 contains preliminaries related to the basics of kinematics for large strain thermo-plasticity and the general form of free energy function. Section 3 presents the governing equations for the (I)BVP, whereas plasticity is briefly described in Section 4. The core section which contains the stability analysis of thermo-elastoplastic material model is Section 5. Firstly, the general model is considered and, secondly, the quasi-static conductive case obtained by dropping the inertial term is analysed. Section 6 contains the specification of the thermo-elastoplastic model and its implementation within FEM. The results of example numerical simulations are described in Section 7, and Section 8 contains final remarks.

In the paper the formulas containing vectors or tensors are written in absolute notation. The definitions of products and derivatives are included in Appendix A.

2. Preliminaries

2.1. Kinematics

Let us assume that vector $\mathbf{X}$ denotes the referential placement of a material particle, and that vector $\mathbf{x}(\mathbf{X}, t)$ is the current placement at time t of the particle labelled with $\mathbf{X}$. The absolute temperature is denoted by T. The displacement vector is defined as the difference

$$\mathbf{u}(\mathbf{X}, t) = \mathbf{x}(\mathbf{X}, t) - \mathbf{X}. \tag{2.1}$$

In further description, the dependence of quantities on the particle referential placement $\mathbf{X}$ and time t is not written directly. The deformation gradient is defined as usual

$$\mathbf{F} = \frac{\partial \mathbf{x}}{\partial \mathbf{X}} = \mathbf{I} + \frac{\partial \mathbf{u}}{\partial \mathbf{X}}, \tag{2.2}$$

where $\mathbf{I}$ is the second-order identity tensor.

The kinematics of the analysed thermo-plasticity model is based on the multiplicative decomposition of the deformation gradient in the following form [48]

$$\mathbf{F} = \mathbf{F}^r \cdot \mathbf{F}^p, \tag{2.3}$$

where $\mathbf{F}^r$ includes the reversible part of deformation (elastic deformation and thermal expansion) and $\mathbf{F}^p$ represents the plastic part. The reversible part can be decomposed into elastic and thermal parts

$$\mathbf{F}^r = \mathbf{F}^\theta \cdot \mathbf{F}^e. \tag{2.4}$$

Assuming isotropic linear expansion, the thermal part of deformation gradient has the form [41]

$$\mathbf{F}^\theta = J^\theta \mathbf{I}, \qquad J^\theta = \exp(3\alpha_T [T - T_0]) \tag{2.5}$$

and the deformation gradient can be expressed in the form

$$\mathbf{F} = J^\theta \mathbf{F}^e \cdot \mathbf{F}^p. \tag{2.6}$$

The right Cauchy–Green deformation tensor is defined as

$$\mathbf{C} = \mathbf{F}^{\mathrm{T}} \cdot \mathbf{F} \tag{2.7}$$

and the elastic right Cauchy–Green tensor is

$$\mathbf{C}^e = [\mathbf{F}^e]^{\mathrm{T}} \cdot \mathbf{F}^e. \tag{2.8}$$

It can be shown that the right elastic Cauchy–Green tensor can be expressed in the form

$$\mathbf{C}^e = [J^\theta]^{-2} [\mathbf{F}^{-p}]^{\mathrm{T}} \cdot \mathbf{C} \cdot \mathbf{F}^{-p}, \tag{2.9}$$

where $\mathbf{F}^{-p} = [\mathbf{F}^p]^{-1}$.

The velocity of a particle is defined in the classical way

$$\mathbf{v} = \frac{\partial \mathbf{x}(\mathbf{X}, t)}{\partial t} = \dot{\mathbf{x}}, \tag{2.10}$$

where the dot over a quantity denotes the material time derivative, see e.g. [49], and is referred to as the rate of a quantity. This notation is used in the subsequent derivations. The velocity gradient is

$$\mathbf{l} = \frac{\partial \mathbf{v}}{\partial \mathbf{x}} = \mathrm{grad}(\mathbf{v}) = \dot{\mathbf{F}} \cdot \mathbf{F}^{-1}. \tag{2.11}$$

2.2. Free energy

In this work the Helmholtz free energy for a thermo-elastoplastic material is assumed to be dependent on deformation gradient $\mathbf{F}$, absolute temperature T and a vector of internal variables related to plasticity $\mathbf{a}$

$$\psi = \psi(\mathbf{F}, T, \mathbf{a}). \tag{2.12}$$

However, the coupled thermo-elastoplastic problem leads to a two-field formulation consisting of two governing equations: the balance of linear momentum and the balance of energy with two unknown fields, namely displacement vector $\mathbf{u}$ and temperature T. In order to find the vector of internal variables the plasticity problem is solved at a local level. Thus vector $\mathbf{a}$ is indeed dependent on the fundamental fields, i.e., $\mathbf{a}(\mathbf{F}(\mathbf{u}(\mathbf{X}, t)), T(\mathbf{X}, t))$ which implies that:

$$\frac{\partial \mathbf{a}}{\partial \mathbf{X}} = \frac{\partial \mathbf{a}}{\partial \mathbf{F}} : \frac{\partial \mathbf{F}}{\partial \mathbf{X}} + \frac{\partial \mathbf{a}}{\partial T} \otimes \frac{\partial T}{\partial \mathbf{X}} = \frac{\partial \mathbf{a}}{\partial \mathbf{F}} : \frac{\partial^2 \mathbf{u}}{\partial \mathbf{X} \partial \mathbf{X}} + \frac{\partial \mathbf{a}}{\partial T} \otimes \frac{\partial T}{\partial \mathbf{X}}, \tag{2.13}$$

$$\dot{\mathbf{a}} = \frac{\partial \mathbf{a}}{\partial \mathbf{F}} : \dot{\mathbf{F}} + \frac{\partial \mathbf{a}}{\partial T} \dot{T} = \frac{\partial \mathbf{a}}{\partial \mathbf{F}} : \frac{\partial^2 \mathbf{u}}{\partial \mathbf{X} \partial t} + \frac{\partial \mathbf{a}}{\partial T} \dot{T}. \tag{2.14}$$

The vector of internal variables $\mathbf{a}$ typically contains the tensor representing plastic deformation and an equivalent plastic strain measure.

3. Governing equations

The subsequent derivations presented in this section are standard and can be found in the literature, e.g., [50, 51].

3.1. The first law of thermodynamics

The first law of thermodynamics, i.e., the energy balance equation, is considered in the reference configuration

$$\rho_0 \dot{e} - \mathbf{P} : \dot{\mathbf{F}} + \mathrm{Div}(\mathbf{q}_0) = 0, \tag{3.1}$$

where ρ_0 is the referential density, e is the internal energy per unit of mass in the reference configuration, $\mathbf{P}$ is the first Piola–Kirchhoff stress tensor, $\mathbf{q}_0$ is the Piola–Kirchhoff heat flux density vector and $\mathrm{Div}(\cdot)$ denotes the divergence in the reference configuration. The balance of energy in Eq. (3.1) does not take into account the external source of heat per unit of mass (or volume).

3.2. The second law of thermodynamics

The second law of thermodynamics states that the energy dissipation $\mathcal{D}$ is always non-negative

$$\mathcal{D} = \mathbf{P} : \dot{\mathbf{F}} - \rho_0 \eta \dot{T} - \rho_0 \dot{\psi} - \frac{1}{T} \mathbf{q}_0 \cdot \mathrm{Grad}(T) \geq 0. \tag{3.2}$$

In the above equation η is the entropy per unit of mass in the reference configuration and $\mathrm{Grad}(\cdot)$ denotes the gradient of a quantity in the reference configuration.

The rate of the Helmholtz free energy density introduced in Eq. (2.12) is derived as follows

$$\dot{\psi} = \frac{\partial \psi}{\partial \mathbf{F}} : \dot{\mathbf{F}} + \frac{\partial \psi}{\partial \mathbf{a}} \cdot \dot{\mathbf{a}} + \frac{\partial \psi}{\partial T} \dot{T}. \tag{3.3}$$

After inserting the above relation into Eq. (3.2) the following inequality is obtained

$$\left[\mathbf{P} - \rho_0 \frac{\partial \psi}{\partial \mathbf{F}} \right] : \dot{\mathbf{F}} - \rho_0 \frac{\partial \psi}{\partial \mathbf{a}} \cdot \dot{\mathbf{a}} - \rho_0 \left[\eta + \frac{\partial \psi}{\partial T} \right] \dot{T} - \frac{1}{T} \mathbf{q}_0 \cdot \mathrm{Grad}(T) \geq 0. \tag{3.4}$$

The following state equations are obtained for the first Piola–Kirchhoff stress tensor and the entropy:

$$\mathbf{P} = \rho_0 \frac{\partial \psi}{\partial \mathbf{F}}, \tag{3.5}$$

$$\eta = -\frac{\partial \psi}{\partial T}. \tag{3.6}$$

The reduced form of the second law of thermodynamics is now written as

$$-\rho_0 \frac{\partial \psi}{\partial \mathbf{a}} \cdot \dot{\mathbf{a}} - \frac{1}{T}\mathbf{q}_0 \cdot \mathrm{Grad}(T) \geq 0. \tag{3.7}$$

By inserting the definition of a thermodynamic force $\boldsymbol{\beta}$ conjugate to $\mathbf{a}$

$$\boldsymbol{\beta} = -\rho_0 \frac{\partial \psi}{\partial \mathbf{a}}, \tag{3.8}$$

the following inequality is obtained

$$\boldsymbol{\beta} \cdot \dot{\mathbf{a}} - \frac{1}{T}\mathbf{q}_0 \cdot \mathrm{Grad}(T) \geq 0, \tag{3.9}$$

in which the two terms are called mechanical and thermal dissipation, respectively:

$$\mathcal{D}_{mech} = \boldsymbol{\beta} \cdot \dot{\mathbf{a}} \geq 0, \tag{3.10}$$

$$\mathcal{D}_{therm} = -\frac{1}{T}\mathbf{q}_0 \cdot \mathrm{Grad}(T) \geq 0. \tag{3.11}$$

The constitutive relation for the heat flux density vector has to be specified. In this work the simplest relation is assumed, i.e., that the Piola–Kirchhoff heat flux density vector is proportional to the material gradient of the temperature field

$$\mathbf{q}_0 = -K\,\mathrm{Grad}(T), \tag{3.12}$$

where $K > 0$ is the heat conductivity parameter. Is is assumed that the material is homogeneous, i.e., K does not depend on $\mathbf{X}$. However, spatial Fourier's law can alternatively be incorporated instead, see [52].

For assumed Fourier's law in Eq. (3.12) the dissipation inequality presented in Eq. (3.11) is fulfilled.

3.3. Temperature form of energy balance

To derive the temperature form of the energy balance equation the Legendre transformation is needed

$$\psi = e - T\eta, \tag{3.13}$$

which implies the following relations:

$$\dot{\psi} = \dot{e} - \dot{T}\eta - T\dot{\eta}, \tag{3.14}$$

$$\dot{e} = \dot{\psi} + \dot{T}\eta + T\dot{\eta}. \tag{3.15}$$

By inserting Eqs. (3.15), (3.3), (3.5), (3.6), (3.8) and (3.12) into the first law of thermodynamics (3.1) and by using relation

$$\dot{\eta} = -\frac{\partial^2 \psi}{\partial T \partial \mathbf{F}} : \dot{\mathbf{F}} - \frac{\partial^2 \psi}{\partial T \partial \mathbf{a}} \cdot \dot{\mathbf{a}} - \frac{\partial^2 \psi}{\partial T^2} \dot{T}, \tag{3.16}$$

the following form of energy balance equation is obtained

$$\rho_0 c \dot{T} - K \operatorname{Div}(\operatorname{Grad}(T)) - \underbrace{T \frac{\partial \mathbf{P}}{\partial T} : \dot{\mathbf{F}}}_{\mathcal{H}} - \underbrace{\boldsymbol{\beta} \cdot \dot{\mathbf{a}}}_{\mathcal{D}_{mech}} + \underbrace{T \frac{\partial \boldsymbol{\beta}}{\partial T} \cdot \dot{\mathbf{a}}}_{\mathcal{F}} = 0. \tag{3.17}$$

In the above formula c denotes the heat capacity per unit of mass defined as

$$c = -T \frac{\partial^2 \psi}{\partial T^2}. \tag{3.18}$$

The mechanical heat production rate in Eq. (3.17) consists of three components. The first is related to thermo-elastic coupling (Gough–Joule effect) and is denoted $\mathcal{H}$. The second, $\mathcal{D}_{mech}$, is the heat production due to plastic yielding and hardening. The third, $\mathcal{F}$, is due to the dependence of thermodynamic forces conjugated to internal variables on temperature.

By inserting Eq. (2.14) and relation $\dot{\mathbf{F}} = \partial \dot{\mathbf{u}} / \partial \mathbf{X}$ into the energy balance equation (3.17) the final form of the energy balance equation, which is used for ellipticity analysis, has been obtained

$$\rho_0 c \dot{T} - K \operatorname{Div}(\operatorname{Grad}(T)) - \left[T \frac{\partial \mathbf{P}}{\partial T} - \mathbf{Q}^{au} \right] : \frac{\partial \dot{\mathbf{u}}}{\partial \mathbf{X}} + q^{aT} \dot{T} = 0, \tag{3.19}$$

where

$$\mathbf{Q}^{au} = \left[-\boldsymbol{\beta} + T \frac{\partial \boldsymbol{\beta}}{\partial T} \right] \cdot \frac{\partial \mathbf{a}}{\partial \mathbf{F}}, \tag{3.20}$$

$$q^{aT} = \left[-\boldsymbol{\beta} + T \frac{\partial \boldsymbol{\beta}}{\partial T} \right] \cdot \frac{\partial \mathbf{a}}{\partial T}. \tag{3.21}$$

3.4. Balance of linear momentum

The balance of linear momentum is formulated in the reference configuration neglecting body forces

$$\operatorname{Div}(\mathbf{P}) = \rho_0 \ddot{\mathbf{u}}. \tag{3.22}$$

Using the dependence $\mathbf{P}(\mathbf{F}, T, \mathbf{a})$ which results from Eqs. (2.12) and (3.5), it can be written that

$$\frac{\partial \mathbf{P}}{\partial \mathbf{F}} \vdots \left[\frac{\partial \mathbf{F}}{\partial \mathbf{X}} \right]^{\mathrm{T}} + \frac{\partial \mathbf{P}}{\partial \mathbf{a}} : \left[\frac{\partial \mathbf{a}}{\partial \mathbf{X}} \right]^{\mathrm{T}} + \frac{\partial \mathbf{P}}{\partial T} \cdot \frac{\partial T}{\partial \mathbf{X}} = \rho_0 \ddot{\mathbf{u}}, \tag{3.23}$$

with $\mathcal{A}\cdot\mathbf{a} = \mathbf{a}\cdot\mathcal{A}^{\mathrm{T}}$ for any third order tensor $\mathcal{A}$ and vector $\mathbf{a}$, i.e., $[\mathcal{A}^{\mathrm{T}}]_{ijk} = [\mathcal{A}]_{kij}$, or equivalently

$$\frac{\partial \mathbf{P}}{\partial \mathbf{F}} \vdots \left[\frac{\partial^2 \mathbf{u}}{\partial \mathbf{X}\partial \mathbf{X}}\right]^{\mathrm{T}} + \frac{\partial \mathbf{P}}{\partial \mathbf{a}} : \left[\frac{\partial \mathbf{a}}{\partial \mathbf{X}}\right]^{\mathrm{T}} + \frac{\partial \mathbf{P}}{\partial T} \cdot \frac{\partial T}{\partial \mathbf{X}} = \rho_0 \ddot{\mathbf{u}}. \tag{3.24}$$

Inserting Eq. (2.13) yields

$$\left[\frac{\partial \mathbf{P}}{\partial \mathbf{F}} + \frac{\partial \mathbf{P}}{\partial \mathbf{a}} \cdot \frac{\partial \mathbf{a}}{\partial \mathbf{F}}\right] \vdots \left[\frac{\partial^2 \mathbf{u}}{\partial \mathbf{X}\partial \mathbf{X}}\right]^{\mathrm{T}} + \left[\frac{\partial \mathbf{P}}{\partial T} + \frac{\partial \mathbf{P}}{\partial \mathbf{a}} \cdot \frac{\partial \mathbf{a}}{\partial T}\right] \cdot \frac{\partial T}{\partial \mathbf{X}} = \rho_0 \ddot{\mathbf{u}}. \tag{3.25}$$

Now the following two tensors are introduced:

$$\mathbb{D} = \frac{\partial \mathbf{P}}{\partial \mathbf{F}} + \frac{\partial \mathbf{P}}{\partial \mathbf{a}} \cdot \frac{\partial \mathbf{a}}{\partial \mathbf{F}}, \tag{3.26}$$

$$\mathbf{B} = \frac{\partial \mathbf{P}}{\partial T} + \frac{\partial \mathbf{P}}{\partial \mathbf{a}} \cdot \frac{\partial \mathbf{a}}{\partial T}. \tag{3.27}$$

The fourth-order tensor $\mathbb{D}$ is called material tangent, whereas $\mathbf{B}$ is a second-order stress-temperature tensor. The final concise form of the momentum balance equation is

$$\mathbb{D} \vdots \left[\frac{\partial^2 \mathbf{u}}{\partial \mathbf{X}\partial \mathbf{X}}\right]^{\mathrm{T}} + \mathbf{B} \cdot \frac{\partial T}{\partial \mathbf{X}} = \rho_0 \ddot{\mathbf{u}}. \tag{3.28}$$

4. Plasticity

In this section the general assumptions of plasticity theory are included, cf. [31]. The yield function F is assumed to be dependent on internal variables $\mathbf{a}$, thermodynamic force vector $\boldsymbol{\beta}$, conjugated to internal variables, and on temperature T. Thus the yield condition is as follows

$$F(\boldsymbol{\beta}, \mathbf{a}, T) \leq 0. \tag{4.1}$$

For the plastic flow the following equalities hold

$$F = 0 \qquad \text{and} \qquad \dot{F} = 0. \tag{4.2}$$

The evolution of internal variables is written as

$$\dot{\mathbf{a}} = \dot{\lambda}\mathbf{N}^p, \tag{4.3}$$

where $\dot{\lambda}$ is a consistency parameter (also denoted as plastic multiplier) and

$$\mathbf{N}^p = \frac{\partial G}{\partial \boldsymbol{\beta}} \tag{4.4}$$

is derived from plastic potential $G = G(\boldsymbol{\beta}, \mathbf{a}, T)$ which, for associated plasticity, is equivalent to the yield function. The Kuhn–Tucker loading-unloading conditions are as usual

$$\dot{\lambda} \geq 0 \quad \text{and} \quad F \leq 0 \quad \text{and} \quad \dot{\lambda} F = 0. \tag{4.5}$$

5. Ellipticity analysis for large strain thermo-plasticity

5.1. General considerations

The subsequent derivations are based on the perturbative approach which was adopted for isothermal problems in, e.g., [8] and [12], and for thermo-mechanical considerations in, e.g., [31] and [35]. In particular, the subsequent analysis can be treated as an extension of the approach presented in [35] for large strain thermo-elasticity to thermo-plasticity.

We assume that in the base state the volume element of the material is uniformly deformed, i.e., $\mathbf{u} = \bar{\mathbf{F}} \cdot \mathbf{X} - \mathbf{X}$, where $\bar{\mathbf{F}}$ is the constant deformation gradient. The temperature in the specimen is then considered to be constant as well, i.e., $T = \bar{T}$.

The following perturbations of the base state are studied:

$$\mathbf{u} = \bar{\mathbf{F}} \cdot \mathbf{X} - \mathbf{X} + \mathbf{u}^{pert}(\mathbf{X}, t), \tag{5.1}$$

$$T = \bar{T} + T^{pert}(\mathbf{X}, t). \tag{5.2}$$

It is worth mentioning that the application of Eqs. (2.13) and (2.14) in the above derivations leads to a formulation based on the primary unknown fields, i.e., displacement and temperature, so that perturbations are imposed only on these fields. This is an original approach for thermo-plasticity, whereas in the literature, e.g., [31], a perturbation is also imposed on the internal variable field.

Now the above relations (5.1) and (5.2) are inserted into the balance of linear momentum (3.28) and the balance of energy (3.19), respectively. The former equation leads to

$$\mathbb{D} \vdots \left[\frac{\partial^2 \mathbf{u}^{pert}}{\partial \mathbf{X} \partial \mathbf{X}}\right]^{\mathrm{T}} + \mathbf{B} \cdot \frac{\partial T^{pert}}{\partial \mathbf{X}} - \rho_0 \ddot{\mathbf{u}}^{pert} = \mathbf{0}, \tag{5.3}$$

where the material tangent $\mathbb{D}$ and the stress-temperature tensor $\mathbf{B}$ are calculated for the base state. Proceeding along the same lines for the energy equation (3.19) results in

$$\rho_0 c \dot{T}^{pert} - K \mathrm{Div}(\mathrm{Grad}(T^{pert})) - \left[T \frac{\partial \mathbf{P}}{\partial T} - \mathbf{Q}^{au}\right] : \frac{\partial \dot{\mathbf{u}}^{pert}}{\partial \mathbf{X}} + q^{aT} \dot{T}^{pert} = 0. \tag{5.4}$$

All quantities in the above equations are calculated for the base state, hence also temperature T refers to $\bar{T}$.

The perturbations superposed on the base state can have the form of exponential harmonic waves. For instance in [53] the following form has been proposed:

$$\mathbf{u}^{pert}(\mathbf{X},t) = \exp(ik\,\mathbf{N}\cdot\mathbf{X} - i\omega t)\hat{\mathbf{u}}, \tag{5.5}$$

$$T^{pert}(\mathbf{X},t) = \exp(ik\,\mathbf{N}\cdot\mathbf{X} - i\omega t)\hat{T}, \tag{5.6}$$

where i is the imaginary unit, k is the wave number (real and positive), $\mathbf{N}$ is a unit vector (of real coefficients) in the reference configuration related to the direction of wave propagation, ω is the angular frequency (possibly complex), $\hat{\mathbf{u}}$ and $\hat{T}$ are constant amplitudes to be determined (possibly complex).

Inserting relations (5.5) and (5.6) into Eq. (5.3), after making use of derivations summarized in Appendix B, the following equation for the balance of linear momentum is obtained

$$\begin{aligned} k^2\mathbb{D}\dddot{:}[\hat{\mathbf{u}}\otimes\mathbf{N}\otimes\mathbf{N}]^{\mathrm{T}} - ik\mathbf{B}\cdot\mathbf{N}\hat{T} &= k^2\mathbb{D}\dddot{:}[\mathbf{N}\otimes\hat{\mathbf{u}}\otimes\mathbf{N}] - ik\mathbf{B}\cdot\mathbf{N}\hat{T} \\ &= \omega^2\rho_0\hat{\mathbf{u}}, \end{aligned} \tag{5.7}$$

which can be written in the following form

$$\left[\mathbf{Q} - \frac{\omega^2\rho_0}{k^2}\mathbf{I}\right]\cdot\hat{\mathbf{u}} - \frac{i}{k}\mathbf{b}\hat{T} = \mathbf{0}, \tag{5.8}$$

where $\mathbf{Q}$ is an acoustic tensor:

$$\mathbf{Q} = [\mathbf{I}\otimes\mathbf{N}] : \mathbb{D}\cdot\mathbf{N}, \tag{5.9}$$

$$Q_{ij} = D_{iJkL}N_JN_L \tag{5.10}$$

and where vector $\mathbf{b}$ is defined as

$$\mathbf{b} = \mathbf{B}\cdot\mathbf{N}. \tag{5.11}$$

Introducing relations (5.5) and (5.6) into Eq. (5.4), after linearization (neglect the second order term, i.e., the product of amplitudes $\hat{\mathbf{u}}$ and $\hat{T}$) and making use of derivations gathered in Appendix B, the following equation for the energy balance is obtained

$$-Tik\tilde{\mathbf{b}}\cdot\hat{\mathbf{u}} + \left[\rho_0 c + \frac{ik^2}{\omega}K + q^{aT}\right]\hat{T} = 0, \tag{5.12}$$

where

$$\tilde{\mathbf{b}} = \tilde{\mathbf{B}} \cdot \mathbf{N}, \tag{5.13}$$

$$\tilde{\mathbf{B}} = \left[\frac{\partial \mathbf{P}}{\partial T} - \frac{1}{T}\mathbf{Q}^{au}\right] = \frac{\partial \mathbf{P}}{\partial T} + \left[\frac{1}{T}\boldsymbol{\beta} - \frac{\partial \boldsymbol{\beta}}{\partial T}\right] \cdot \frac{\partial \mathbf{a}}{\partial \mathbf{F}}. \tag{5.14}$$

Equations (5.8) and (5.12) form a system of equations which can be presented by using matrix notation

$$\begin{bmatrix} \mathbf{Q} - \dfrac{\omega^2 \rho_0}{k^2}\mathbf{I} & -\dfrac{i}{k}\mathbf{b} \\ -Tik\tilde{\mathbf{b}} & \rho_0 c + \dfrac{ik^2}{\omega}K + q^{aT} \end{bmatrix} \cdot \begin{bmatrix} \hat{\mathbf{u}} \\ \hat{T} \end{bmatrix} = \begin{bmatrix} \mathbf{0} \\ 0 \end{bmatrix}. \tag{5.15}$$

The thermo-plastic material is called stable if all solutions $\hat{\mathbf{u}}$ and $\hat{T}$ of the set of equations (5.15) are *bounded as* $t \to \infty$ for every choice of the base state defined by ($\bar{\mathbf{F}}$, $\bar{T}$), and for every wave number $k > 0$ and vector $\mathbf{N}$, cf. [35]. The non-trivial solution of system (5.15) is obtained when the determinant of the coefficients matrix is zero

$$\det\left(\begin{bmatrix} \mathbf{Q} - \dfrac{\omega^2 \rho_0}{k^2}\mathbf{I} & -\dfrac{i}{k}\mathbf{b} \\ -Tik\tilde{\mathbf{b}} & \rho_0 c + \dfrac{ik^2}{\omega}K + q^{aT} \end{bmatrix}\right) = 0. \tag{5.16}$$

The amplitudes $\hat{\mathbf{u}}$ and $\hat{T}$ assumed in Eqs. (5.5) and (5.6) are bounded for $t \to \infty$ if

$$\mathrm{Im}(\omega) \leq 0. \tag{5.17}$$

It can therefore be concluded that the material is stable if the condition in Eq. (5.16) is fulfilled for every base state $\bar{\mathbf{F}}$ and $\bar{T}$, wave number $k > 0$ and direction $\mathbf{N}$ and when condition (5.17) holds.

A further analysis of the stability condition is now shown. The amplitude $\hat{T}$ can be derived from Eq. (5.12) as follows

$$\hat{T} = \frac{Tik}{\rho_0 c + \dfrac{ik^2}{\omega}K + q^{aT}}\tilde{\mathbf{b}} \cdot \hat{\mathbf{u}}, \tag{5.18}$$

assuming that the denominator in the fraction is other than 0, and can be inserted into Eq. (5.8). The reduced set of equations is presented below

$$\left[\mathbf{Q} - \frac{\omega^2 \rho_0}{k^2}\mathbf{I} + \frac{T}{\rho_0 c + \dfrac{ik^2}{\omega}K + q^{aT}}\mathbf{b} \otimes \tilde{\mathbf{b}}\right] \cdot \hat{\mathbf{u}} = \mathbf{0}. \tag{5.19}$$

The non-trivial solution of the above equation for $\hat{\mathbf{u}}$ is obtained when

$$\det\left(\mathbf{Q} - \frac{\omega^2\rho_0}{k^2}\mathbf{I} + \frac{T}{\rho_0 c + \dfrac{ik^2}{\omega}K + q^{aT}}\mathbf{b}\otimes\tilde{\mathbf{b}}\right) = 0. \tag{5.20}$$

It is mentioned that the same result, i.e., the derivation of Eq. (5.20) from Eq. (5.16), can be obtained using the formula for the determinant of a block matrix, see, e.g., [54].

5.2. Quasi-static conductive case

A further analysis is performed for quasi-static conditions which are obtained owing to the assumption that in the balance of linear momentum (3.28) the right hand side is zero, so that the term $\omega^2\rho_0/k^2\mathbf{I}$ in Eq. (5.20) is dropped, and Eq. (5.20) reduces to

$$\det\left(\mathbf{Q} + \frac{T}{\rho_0 c + \dfrac{ik^2}{\omega}K + q^{aT}}\mathbf{b}\otimes\tilde{\mathbf{b}}\right) = 0. \tag{5.21}$$

It can be seen that in the above equation the angular frequency ω appears only once and is involved in the conductivity term. Note that this term disappears for the adiabatic model, thus it can be concluded that the presence of heat conductivity in the material model changes the type of the equation and its analysis.

The next step is performed under the assumption that the elastoplastic material tangent is not singular. By application of the formula $\det(\mathbf{T} + \alpha\mathbf{a}\otimes\mathbf{c}) = \det(\mathbf{T})[1 + \alpha\mathbf{c}\cdot\mathbf{T}^{-1}\cdot\mathbf{a}]$, where $\mathbf{T}$ is a second order tensor, α is a scalar and $\mathbf{a}$ and $\mathbf{c}$ are vectors, Eq. (5.21) can be rewritten as

$$\det(\mathbf{Q})\left[1 + \frac{T}{\rho_0 c + \dfrac{ik^2}{\omega}K + q^{aT}}\tilde{\mathbf{b}}\cdot\mathbf{Q}^{-1}\cdot\mathbf{b}\right] = 0. \tag{5.22}$$

The above formula can be considered only for the case where the acoustic tensor $\mathbf{Q}$ is non-singular, so it is fulfilled when

$$1 + \frac{T}{\rho_0 c + \dfrac{ik^2}{\omega}K + q^{aT}}\tilde{\mathbf{b}}\cdot\mathbf{Q}^{-1}\cdot\mathbf{b} = 0. \tag{5.23}$$

Now the angular frequency ω is analysed in order to verify the condition from Eq. (5.17). In this regard, Eq. (5.23) can be rewritten after simple manipulations

$$\omega = \frac{-ik^2K}{\rho_0 c + q^{aT} + T\tilde{\mathbf{b}}\cdot\mathbf{Q}^{-1}\cdot\mathbf{b}}. \tag{5.24}$$

For real values of the wave number k the angular frequency ω has only the imaginary part which equals

$$\mathrm{Im}(\omega) = \frac{-k^2 K}{\rho_0 c + q^{aT} + T\tilde{\mathbf{b}} \cdot \mathbf{Q}^{-1} \cdot \mathbf{b}}. \tag{5.25}$$

Now the condition from Eq. (5.17) is recalled and is applied to Eq. (5.25), which gives

$$\rho_0 c + q^{aT} + T\tilde{\mathbf{b}} \cdot \mathbf{Q}^{-1} \cdot \mathbf{b} \geq 0, \tag{5.26}$$

since k^2 and conductivity K are always positive. It can be concluded that, for the quasi-static conductive case, the stability of the material depends on heat capacity, thermo-plastic coupling (i.e., the dependence of the internal variables and conjugated forces on temperature is represented by term q^{aT}), on thermo-elastic coupling (represented by vectors $\tilde{\mathbf{b}}$ and $\mathbf{b}$) and material tangent (used for the calculation of acoustic tensor $\mathbf{Q}$).

Equation (5.26) can be rewritten in the following form, defining stability indicator S

$$S = T\tilde{\mathbf{b}}(\mathbf{N}) \cdot [\mathbf{Q}(\mathbf{N})]^{-1} \cdot \mathbf{b}(\mathbf{N}) + \rho_0 c + q^{aT} \geq 0 \tag{5.27}$$

to emphasize the dependence of $\tilde{\mathbf{b}}$, $\mathbf{b}$ and $\mathbf{Q}$ on the vector $\mathbf{N}$. The condition presented in Eq. (5.27) can be investigated numerically by seeking the minimum value of the first term with respect to the vector $\mathbf{N}$ and by verification of the sign of the minimum value plus heat capacity and q^{aT}. The negative sign of the expression means that the stability is lost. For classic materials the heat capacity is positive and thus has a stabilizing effect. On the other hand, the thermo-plastic coupling term q^{aT} can be negative for example when thermal softening occurs, which is usually observed for metals.

The stability criterion does not depend straightforwardly on the conductivity. The value of the conductivity coefficient is absent in the condition presented in Eq. (5.27). As mentioned above, the presence of the conductive term just changes the type of the equation to be solved and leads to the condition (5.27).

In the next section the numerical analysis of the above condition is performed. It should be mentioned that from the numerical point of view it makes no sense to consider the case of singular acoustic tensor $\det(\mathbf{Q}) = 0$, which implies that the condition (5.27) cannot be verified. In computer simulations for discretized time and space the determinant of the acoustic tensor is not the analytical zero. Even when the determinant of the acoustic tensor $\mathbf{Q}$ is negative, the stability condition (5.27) can be fulfilled due to the presence of additional terms in the equation.

6. Model specification – large strain thermo-elastoplasticity

6.1. Constitutive relations

The following specific form of the free energy functional is assumed in the paper

$$\psi(\mathbf{F}, \mathbf{a}, T) = \hat{\psi}(\mathbf{F}, \mathbf{F}^p, \alpha, T) \tag{6.1}$$

and thus the internal variables consist of coefficients of the plastic deformation gradient $\mathbf{F}^p$ and the hardening variable α, i.e.,

$$\mathbf{a} = \{\mathbf{F}^p, \alpha\}. \tag{6.2}$$

In the above equation parentheses $\{\cdot\}$ denote vectorization of the related quantities, to be specific $\mathbf{a} = [F^p_{11}, F^p_{12}, F^p_{13}, F^p_{21}, F^p_{22}, F^p_{23}, F^p_{31}, F^p_{32}, F^p_{33}, \alpha]$. Using the definition of the elastic right Cauchy–Green deformation tensor in Eq. (2.8) and relation (2.9) the free energy can be rewritten as

$$\psi(\mathbf{F}, \mathbf{a}, T) = \tilde{\psi}(\mathbf{C}^e(\mathbf{F}, \mathbf{F}^p, T), \alpha, T). \tag{6.3}$$

The free energy is assumed to be composed of elastic, plastic and pure thermal parts as follows, cf. [55],

$$\tilde{\psi} = \psi^e(\mathbf{C}^e) + \psi^p(\alpha) + \psi^\theta(T), \tag{6.4}$$

$$\psi^e(\mathbf{C}^e) = \frac{1}{2\rho_0}\kappa\left[\frac{1}{2}\left[[J^e]^2 - 1\right] - \ln(J^e)\right] + \frac{1}{2\rho_0}G\left[[J^e]^{-2/3}\,\mathrm{tr}(\mathbf{C}^e) - 3\right], \tag{6.5}$$

$$\psi^p(\alpha) = \frac{1}{2}H\alpha^2 + [\sigma_{y\infty} - \sigma_{y0}]\left[\alpha + \frac{1}{\delta}\exp(-\delta\alpha)\right], \tag{6.6}$$

$$\psi^T(T) = c_0\left[[T - T_0] - T\ln\left(\frac{T}{T_0}\right)\right]. \tag{6.7}$$

In the elastic part $J^e > 0$ is the determinant of the elastic deformation tensor $\mathbf{F}^e$. The material parameters in Eq. (6.5) are the bulk modulus κ and the shear modulus G. The plastic part of free energy (6.6) is assumed in a form composed of linear hardening with hardening modulus H, and saturation hardening with initial and final yield thresholds σ_{y0} and $\sigma_{y\infty}$, respectively, and saturation constant δ. Softening can be obtained by using a certain set of parameters (e.g., negative value of H). In Eq. (6.7) parameter c_0 is the specific heat capacity per unit of mass for the selected material. The assumed form of the thermal part of the free energy function implies constant heat capacity derived in Eq. (3.18).

Using Eq. (3.5) the first Piola–Kirchhoff stress tensor can be derived

$$\mathbf{P} = \rho_0\frac{\partial\psi}{\partial\mathbf{F}} = \rho_0\frac{\partial\psi}{\partial\mathbf{C}^e} : \frac{\partial\mathbf{C}^e}{\partial\mathbf{F}} = \rho_0\frac{\partial\psi}{\partial\mathbf{C}^e} : \left[\frac{\partial\mathbf{C}^e}{\partial\mathbf{C}} : \frac{\partial\mathbf{C}}{\partial\mathbf{F}}\right]. \tag{6.8}$$

After manipulations it has the form

$$\mathbf{P} = 2\frac{\rho_0}{J^\theta}\mathbf{F}^e \cdot \frac{\partial \psi}{\partial \mathbf{C}^e} \cdot \left[\mathbf{F}^{-p}\right]^{\mathrm{T}}. \tag{6.9}$$

Introducing the definition of the elastic second Piola–Kirchhoff stress tensor

$$\mathbf{S}^e = 2\rho_0 \frac{\partial \psi}{\partial \mathbf{C}^e}, \tag{6.10}$$

the following form of the first Piola–Kirchhoff stress tensor is obtained

$$\mathbf{P} = \frac{1}{J^\theta}\mathbf{F}^e \cdot \mathbf{S}^e \cdot \left[\mathbf{F}^{-p}\right]^{\mathrm{T}} \quad \Rightarrow \quad J^\theta \mathbf{F}^{-e} \cdot \mathbf{P} = \mathbf{S}^e \cdot \left[\mathbf{F}^{-p}\right]^{\mathrm{T}}. \tag{6.11}$$

Taking into account the definition of $\boldsymbol{\beta}$ in Eq. (3.8) and assumption (6.2), the conjugate forces $\boldsymbol{\beta}$ include

$$\boldsymbol{\beta} = \left\{ -\rho_0 \frac{\partial \psi}{\partial \mathbf{F}^p}, -\rho_0 \frac{\partial \psi}{\partial \alpha} \right\} = \left\{ \boldsymbol{\beta}^p, \beta^\alpha \right\}. \tag{6.12}$$

Further derivations yield

$$\boldsymbol{\beta}^p = -\rho_0 \frac{\partial \psi}{\partial \mathbf{C}^e} : \frac{\partial \mathbf{C}^e}{\partial \mathbf{F}^p} = -\rho_0 \frac{\partial \psi}{\partial \mathbf{C}^e} : \left[\frac{\partial \mathbf{C}^e}{\partial \mathbf{F}^{-p}} : \frac{\partial \mathbf{F}^{-p}}{\partial \mathbf{F}^p} \right] \tag{6.13}$$

and

$$\boldsymbol{\beta}^p = 2\rho_0 \mathbf{C}^e \cdot \frac{\partial \psi}{\partial \mathbf{C}^e} \cdot \left[\mathbf{F}^{-p}\right]^{\mathrm{T}} = \mathbf{C}^e \cdot \mathbf{S}^e \cdot \left[\mathbf{F}^{-p}\right]^{\mathrm{T}} = \mathbf{M} \cdot \left[\mathbf{F}^{-p}\right]^{\mathrm{T}}, \tag{6.14}$$

where $\mathbf{M}$ is the (elastic) Mandel stress tensor

$$\mathbf{M} = \mathbf{C}^e \cdot \mathbf{S}^e = 2\rho_0 \mathbf{C}^e \cdot \frac{\partial \psi}{\partial \mathbf{C}^e}, \tag{6.15}$$

which is symmetric in the case of elastic isotropy. Moreover, the definition of the second conjugate force results in

$$\beta^\alpha = -\rho_0 \frac{\partial \psi}{\partial \alpha} = -\left[H\alpha + [\sigma_{y\infty} - \sigma_{y0}][1 - \exp(-\delta\alpha)] \right]. \tag{6.16}$$

With these relations in hand, the mechanical dissipation according to Eq. (3.10) reads

$$\begin{aligned} \mathcal{D}_{mech} &= \boldsymbol{\beta}^p : \dot{\mathbf{F}}^p + \beta^\alpha \dot{\alpha} = \left[\mathbf{M} \cdot [\mathbf{F}^{-p}]^{\mathrm{T}}\right] : \dot{\mathbf{F}}^p + \beta^\alpha \dot{\alpha} \\ &= \mathbf{M} : [\dot{\mathbf{F}}^p \cdot \mathbf{F}^{-p}] + \beta^\alpha \dot{\alpha} = \mathbf{M} : \mathbf{L}^p + \beta^\alpha \dot{\alpha}. \end{aligned} \tag{6.17}$$

Furthermore, the yield condition according to Eq. (4.1)

$$F = F(\boldsymbol{\beta}, \mathbf{a}, T) = F(\boldsymbol{\beta}^p, \beta^\alpha, \mathbf{F}^p, \alpha, T) = \tilde{F}(\mathbf{M}, \beta^\alpha, T) \leq 0 \tag{6.18}$$

is assumed in the following specific form

$$F = \|\mathrm{dev}(\mathbf{M})\| - \sqrt{\frac{2}{3}}\sigma_y(\alpha, T) \leq 0, \tag{6.19}$$

where

$$\mathrm{dev}(\mathbf{M}) = \mathbf{M} - \frac{1}{3}\mathrm{tr}\,(\mathbf{M})\,\mathbf{I}, \qquad \|\mathrm{dev}(\mathbf{M})\| = \sqrt{\mathrm{dev}(\mathbf{M}) : \mathrm{dev}(\mathbf{M})} \tag{6.20}$$

and

$$\sigma_y(\alpha, T) = [\sigma_{y0} - \beta^\alpha]\,[1 - H_T[T - T_0]]\,. \tag{6.21}$$

In the model it is assumed that the yield strength is reduced with the increase of temperature. In Eq. (6.21) symbol $H_T > 0$ denotes the linear thermal softening modulus.

The evolution of internal variables for associated plasticity according to Eq. (4.3) is governed by the following equations:

$$\dot{\mathbf{F}}^p = \dot{\lambda}\frac{\partial F}{\partial \boldsymbol{\beta}^p} = \dot{\lambda}\frac{\partial F}{\partial \mathbf{M}} : \frac{\partial \mathbf{M}}{\partial \boldsymbol{\beta}^p} = \dot{\lambda}\frac{\partial F}{\partial \mathbf{M}} \cdot \mathbf{F}^p \iff \dot{\mathbf{F}}^p \cdot \mathbf{F}^{-p} = \mathbf{L}^p = \dot{\lambda}\frac{\partial F}{\partial \mathbf{M}}, \tag{6.22}$$

$$\dot{\alpha} = \dot{\lambda}\frac{\partial F}{\partial \beta^\alpha}. \tag{6.23}$$

Using the yield function from Eq. (6.19) the evolution equations have the form:

$$\mathbf{L}^p = \dot{\lambda}\frac{\partial F}{\partial \mathbf{M}} = \dot{\lambda}\frac{\mathrm{dev}(\mathbf{M})}{\|\mathrm{dev}(\mathbf{M})\|} = \dot{\lambda}\mathbf{N}^p, \tag{6.24}$$

$$\dot{\alpha} = \dot{\lambda}\frac{\partial F}{\partial \beta^\alpha} = \sqrt{\frac{2}{3}}\dot{\lambda}. \tag{6.25}$$

6.2. Numerical implementation of elastoplasticity

The material model presented in the previous section is implemented within the FEM by using symbolic-numerical toolboxes *AceGen* and *AceFEM* [47] for *Wolfram Mathematica*. It should be emphasized that the analysed problem is highly nonlinear due to large deformations, plastic behaviour, and full thermo-mechanical coupling, and that the FEM leads to a set of nonlinear equations which are solved by using the incremental-iterative Newton–Raphson procedure.

From this point of view, the applied software has the capability of Automatic Differentiation (AD), which allows the computation of the tangent matrix for the Newton–Raphson algorithm. This is the most challenging task for advanced nonlinear models. The *AceGen* package also has the capability of simultaneous optimization of expressions immediately after they have been derived, which results in an efficient code for FEM computations, see [47].

The solution algorithm is developed in a form which takes advantage of the capabilities of AceGen package, i.e., symbolic notation and AD (with exceptions when needed, see [47]). The part of the algorithm related to the solution of the plasticity problem at a Gauss point is based on the approach presented in [56] and [47], whereas the implementation of a simpler model of thermo-plasticity is presented in [45].

As mentioned in Section 2.2, the thermo-mechanical problem consists of two governing equations: the balance of linear momentum and the balance of energy, with the local forms presented in Eqs. (3.22) and (3.19), respectively. Following recommendations from [47], for each governing equation a potential (or pseudo-potential) is formulated in such a way that the variation of the potential is equivalent to the weak form of the governing equation. In particular, the density of potential for the balance of linear momentum is the elastic part of the Helmholtz free energy ψ^e from Eq. (6.5), whereas the density of pseudo-potential for the energy balance (3.17) has the following form (using the backward Euler scheme for a temperature rate with T_n denoting the temperature at the previous time moment)

$$\Pi = \frac{1}{2}\rho_0 c\frac{[T-T_n]^2}{\Delta t} + \frac{1}{2}K\mathrm{Grad}(T)\cdot\mathrm{Grad}(T) - T[\mathcal{D}_{mech} + \mathcal{H} - \mathcal{F}]. \tag{6.26}$$

The two discretized fields in the analysed model are displacements $\mathbf{u}$ and temperature T which are interpolated by using linear shape functions. To avoid volumetric locking, which can influence the results for incompressible Huber–Mises plasticity, the so-called *F-bar* modification proposed in [57] is applied. The nodal coefficients of the displacement vector for a finite element are included in the vector $\mathbf{u}_I$, whereas the nodal temperatures are gathered in vector $\mathbf{T}_I$.

The Gauss point contributions to the residual vector $\mathbf{R}_G = \{\mathbf{R}_u, \mathbf{R}_T\}$ are computed as follows

$$\mathbf{R}_u = w_G J_{XG}\left.\frac{\partial\psi^e}{\partial\mathbf{u}_I}\right|_{\mathbf{a}=\mathrm{const}} \tag{6.27}$$

and

$$\mathbf{R}_T = w_G J_{XG}\left.\frac{\partial\Pi}{\partial\mathbf{T}_I}\right|_{\mathbf{a}=\mathrm{const},\,\mathcal{D}_{mech}=\mathrm{const},\,\mathcal{H}=\mathrm{const},\,\mathcal{F}=\mathrm{const}}, \tag{6.28}$$

where w_G is the weight of a Gauss point, J_{XG} denotes the Jacobian of isoparametric mapping from the parent element to the element in the reference configuration. The assumption that the heat sources are constant guarantees correct derivation of the residual vector from the proposed potential (6.26) and is achieved by the application of AD exceptions, whereas constant internal variables **a** prevent the application of nested dependencies calculated in the inner plasticity loop. The Gauss point contribution to the tangent matrix is computed by using AD from the formula

$$\mathbf{K}_G = \begin{bmatrix} \dfrac{\partial \mathbf{R}_u}{\partial \mathbf{u}_I} & \dfrac{\partial \mathbf{R}_u}{\partial \mathbf{T}_I} \\ \dfrac{\partial \mathbf{R}_T}{\partial \mathbf{u}_I} & \dfrac{\partial \mathbf{R}_T}{\partial \mathbf{T}_I} \end{bmatrix} = \begin{bmatrix} \mathbf{K}_{uu} & \mathbf{K}_{uT} \\ \mathbf{K}_{Tu} & \mathbf{K}_{TT} \end{bmatrix}. \tag{6.29}$$

The solution algorithm is presented in Box 1.

The important aspect of the elastoplasticity problem is its solution at the Gauss point level. If the calculation of a trial state results in a plastic state, see point 3 in Box 1, then the set of nonlinear equations consisting of the yield condition and the flow rule has to be solved in order to find values of the internal variables. To keep consequently the analysis in the referential setting the following algorithm is developed:

The flow rule (6.22) to be solved can be rewritten as

$$\dot{\mathbf{F}}^p = \dot{\lambda}\mathbf{N} \cdot \mathbf{F}^p \tag{6.30}$$

and can be approximated by using exponential mapping discussed in [58]. The application of formula (45) from [58] for Eq. (6.30) gives

$$\mathbf{F}^p_{n+1} = \exp(\Delta t[\dot{\lambda}\mathbf{N}^p]_{n+1}) \cdot \mathbf{F}^p_n, \tag{6.31}$$

where Δt denotes the time increment and subscripts n and $n+1$ denote the values from the previous and the current time step, respectively. In the subsequent derivations, subscripts $n+1$ related to the current step are omitted. Assuming backward Euler integration with $\dot{\lambda} = \Delta\lambda/\Delta t$, the above formula is rewritten in the residual form

$$\mathbf{F}^p - \exp(\Delta\lambda\mathbf{N}^p) \cdot \mathbf{F}^p_n = \mathbf{0}. \tag{6.32}$$

It is worth noting that the solution of the plasticity problem at the level of a Gauss point, see point 3 in Box 1, can be performed using an alternative approach presented for instance in [50], including the analysis in principal directions, which reduces the number of unknowns. However, in the presented model it is assumed that the vector of internal variables is calculated straightforwardly,

which allows for the computation of derivatives $\partial\mathbf{a}/\partial\mathbf{F}$ and $\partial\mathbf{a}/\partial T$, required to compute quantities $\tilde{\mathbf{B}}$ and $\mathbf{q}^{aT}$ in Eqs. (5.14) and (5.27) in an automated manner, cf. [47, Subsection 3.3.1]. This is also mentioned in the last line of point 3 in Box 1. Moreover, the presented framework is already prepared for a possible extension towards anisotropic plastic flow in future research.

- Current values of fundamental unknowns: vector of nodal displacements $\mathbf{u}_I$, vector of nodal temperatures $\mathbf{T}_I$
- Previous values of fundamental unknowns: $\mathbf{u}_{nI}$, $\mathbf{T}_{nI}$
- Interpolation using shape functions: $\mathbf{u} = \mathbf{N}_{u,I} \cdot \mathbf{u}_I$, $T = \mathbf{N}_{T,I} \cdot \mathbf{T}_I$, $\mathbf{u}_n = \mathbf{N}_{u,I} \cdot \mathbf{u}_{nI}$, $T_n = \mathbf{N}_{T,I} \cdot \mathbf{T}_{nI}$
- Values of internal variables at Gauss points from previous time step: $\mathbf{F}_n^{-p}$, α_n
- Loop over Gauss points to calculate contributions to residual vector and tangent matrix:
  1. Calculation of trial state:
     $\mathbf{F}$ from Eq. (2.2), $\mathbf{F}^\theta$ from Eq. (2.5)
     $\mathbf{F}^{e,trial} = \mathbf{F}^{-\theta} \cdot \mathbf{F} \cdot \mathbf{F}_n^{-p}$ $\quad$ $\mathbf{C}^{e,trial} = [\mathbf{F}^{e,trial}]^{\mathrm{T}} \cdot \mathbf{F}^{e,trial}$
     $\psi^{e,trial}(\mathbf{C}^{e,trial})$ from Eq. (6.5)
     $\mathbf{M}^{trial} = 2\mathbf{C}^{e,trial} \cdot \partial\psi^{e,trial}/\partial\mathbf{C}^{e,trial}$
     $F^{trial}(\mathbf{M}^{trial}, \beta^\alpha(\alpha_n), T)$ from Eq. (6.19)
  2. If $F^{trial} < \epsilon$ then elastic state, $\mathbf{F}^p = \mathbf{F}_n^p$, $\alpha = \alpha_n$
  3. If $F^{trial} \geq \epsilon$ then plastic state, the following set of equations is solved by Newton's method:
     $$\begin{cases} F = 0 \\ \mathbf{F}^p - \exp(\sqrt{3/2}[\alpha - \alpha_n]\mathbf{N}^p) \cdot \mathbf{F}_n^p = \mathbf{0} \end{cases}$$
     to obtain $\mathbf{F}^p$ and α.
     When the solution is obtained, the dependencies needed for linearization are included in quantities:
     $$\mathbf{F}^p = \mathbf{F}^p\big|_{\frac{\partial\mathbf{F}^p}{\partial\mathbf{F}} = DFpDF,\ \frac{\partial\mathbf{F}^p}{\partial T} = DFpDT}$$
     $$\alpha = \alpha\big|_{\frac{\partial\alpha}{\partial\mathbf{F}} = D\alpha DF,\ \frac{\partial\alpha}{\partial T} = D\alpha DT}$$
     Derivatives $DFpDF$, $DFpDT$, $D\alpha DF$ and $D\alpha DT$ are calculated after convergent step in the inner Newton procedure
  4. Calculation of final value of $\mathbf{C}^e$ from Eq. (2.9) and free energy function from Eq. (6.5)
  5. Calculation of internal heat sources due to thermo-elastic and thermo-plastic couplings from Eq. (3.17)
  6. Calculation of data needed for stability condition (5.27), i.e., $\tilde{\mathbf{B}}$ from Eq. (5.14), $\mathbb{D}$ from Eq. (3.26), $\mathbf{B}$ from Eq. (3.27) and q^{aT} from Eq. (3.21), and saving them in finite element database
  7. Calculation of pseudo potential Π for energy balance from Eq. (6.26)
  8. Computation of Gauss point contributions to residual vector and tangent matrix from Eqs. (6.27) and (6.28)

Box 1. Flowchart of AceGen solution algorithm for thermo-elastoplasticity.

By using relation (6.25) the above equation can be expressed as

$$\mathbf{F}^p - \exp\left(\sqrt{\frac{3}{2}}[\alpha - \alpha_n]\mathbf{N}^p\right) \cdot \mathbf{F}_n^p = \mathbf{0}. \tag{6.33}$$

To conclude, the problem to be solved consists of 10 unknowns (i.e., nine components of $\mathbf{F}^p$ and α) and 10 equations, namely 9 equations presented in Eq. (6.33) and the plasticity criterion (6.19).

Another crucial aspect of the plasticity solution is its linearization. After a convergent step of the inner loop the derivatives of internal variables with respect to the deformation gradient and temperature are calculated by using the method presented in [47, Subsection 3.3.1]. The derivatives are also used in this paper for the calculation of quantities involved in the stability condition: q^{aT} from Eq. (3.21), material tangent $\mathbb{D}$ from Eq. (3.26) and stress–temperature tensor $\mathbf{B}$ from Eq. (3.27). At the end of a convergent step the quantities related to the stability condition are saved in the finite element database and can be used for verification at a selected Gauss point, after a time step of the simulation.

7. Numerical analysis of stability condition for quasi-static conductive case

The aim of this section is to present the numerical analysis of the derived condition for quasi-static thermo-elastoplasticity, cf. Eq. (5.27). The analysis is performed for three-dimensional configurations, in particular a homogenous deformation of a cube under simple shear and tension of a plate with an imperfection are simulated with the material model presented in the previous section. At selected Gauss points and load steps the verification of the condition is performed by seeking the minimum of the left-hand side of Eq. (5.27) for the discretized vector $\mathbf{N}$ which is described in spherical coordinates by using the two angles α and β

$$\mathbf{N} = \cos(\alpha)\cos(\beta)\,\mathbf{e}_1 + \sin(\alpha)\cos(\beta)\,\mathbf{e}_2 + \sin(\beta)\,\mathbf{e}_3 \tag{7.1}$$

with orthonormal base system $\{\mathbf{e}_1, \mathbf{e}_2, \mathbf{e}_3\}$. The angle α is discretized in range $[0, \pi]$ and angle β in range $[0, \pi/2]$ with increment $\pi/360$ (i.e., 0.5 deg).

For the analysed values of the angles α and β the left hand side of Eq. (5.27), i.e., the value of variable S, is calculated. It is checked if the value is greater than zero. In addition, the sign of the determinant of the acoustic tensor $\det(\mathbf{Q})$ is verified. Pilot results for the numerical analysis of an elastoplastic tensioned plate with an imperfection under plane strain or plane stress and isothermal conditions were presented in [59].

Material parameters related to elasticity and thermal properties, used in the simulations, are based on steel properties and are included in Table 1. Plasticity parameters differ between tests and are provided in the subsequent subsections. Note that the set of basic units includes mm for length and kN for force, which implies GPa for pressure, respectively stresses. The value of tolerance for verification of the trial state, see points 2 and 3 in Box 1, is assumed to be equal to $\epsilon = 10^{-8}$ GPa.

Table 1. Elastic and thermal material parameters.

Property	Symbol	Value	Unit
Bulk modulus	κ	164.28	GPa
Shear modulus	G	80.23	GPa
Thermal expansion coefficient	α_T	$23.2 \cdot 10^{-6}$	K^{-1}
Heat capacity	$\rho_0 c$	0.00345	GPa/K
Heat conductivity	K	0.121	kN/[Ks]

Numerical simulations of a softening material can result in a pathological mesh dependence which can be an indicator of the loss of stability of a specimen. In turn, the loss of stability at a material point (or points) is a precursor of the loss of stability of the whole structural model. However, the main focus of the paper is not to provide a regularization framework (even though sufficient heat conductivity can contribute to the regularization), but to provide an indicator for thermo-plasticity when material stability is lost at the local level, i.e., at a material point. Therefore, the mesh dependence is not investigated in the paper, instead simulations are carried out with one selected mesh for each test.

It is worth mentioning that the first test elaborated in Section 7.1, i.e., simple shearing of a specimen, simulated with one finite element, results in a uniform stress state. Using a finer discretization would (depending on the specification of boundary conditions) result in a different (inhomogeneous) form of deformation, and thus there would be no point in comparing the results.

7.1. Homogeneous deformation under simple shear

The first test is performed for one cubic finite element in the simple shear state presented in Fig. 1. The dimensions of the cube are $10 \times 10 \times 10$ mm, the enforced displacement ΔL is applied with a uniform rate equal to 0.05 mm/s. The initial temperature of the sample is $T_0 = 297.15$ K and zero natural boundary conditions are assumed for the temperature field (insulation). An adaptive time stepping, provided in AceFEM package [60], is applied in the simulations. The parameters of the time stepping are as follows: the first time step is 10^{-2} s, the minimum and maximum time increments are 10^{-3} s and 10^{-1} s, respectively. The process lasts 100 s.

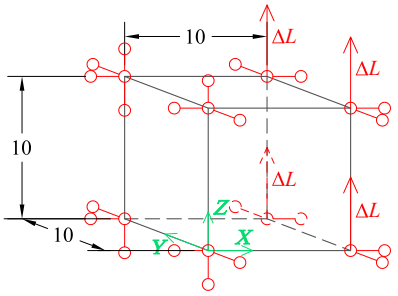

Fig. 1. One cubic finite element under simple shear, dimensions are in mm.

The sample undergoes exponential hardening defined by parameters: $\sigma_{y0} = 0.3$ GPa, $\sigma_{y\infty} = 0.45$ GPa and $\delta = 16.93$ in Eq. (6.16), and softening caused by thermal or material sources. In particular, the sample is analysed twice:

- *Test 1* – material undergoes linear thermal softening with the thermal softening modulus $H_T = 0.02$ K^{-1} in Eq. (6.21) (linear hardening/softening is inactive, i.e., $H = 0$ in Eq. (6.16));
- *Test 2* – material undergoes linear material softening, with $H = -0.621$ GPa in Eq. (6.16), without thermal softening, i.e., $H_T = 0$ in Eq. (6.21).

The summary of plasticity parameters for Test 1 and Test 2 is provided in Tables 2 and 3, respectively.

Table 2. Plasticity parameters for Test 1.

Property	Symbol	Value	Unit
Initial yield threshold	σ_{y0}	0.3	GPa
Final yield threshold	$\sigma_{y\infty}$	0.45	GPa
Saturation constant	δ	16.93	–
Hardening modulus	H	0	GPa
Thermal softening modulus	H_T	0.02	K^{-1}

Table 3. Plasticity parameters for Test 2.

Property	Symbol	Value	Unit
Initial yield threshold	σ_{y0}	0.3	GPa
Final yield threshold	$\sigma_{y\infty}$	0.45	GPa
Saturation constant	δ	16.93	–
Hardening modulus	H	−0.621	GPa
Thermal softening modulus	H_T	0	K^{-1}

The aim of the analysis is to check whether the source of softening, either material or thermal, influences the stability condition derived in Eq. (5.27).

The response of the sample in Test 1 is presented in Fig. 2. It can be observed from the reaction diagram in Fig. 2a that in the plastic regime the initial hardening is followed by the decrease of reaction sum due to thermal softening. The temperature in the sample increases due to plastic heating. It should be noted that, although heat conductivity is activated in this test, it has no influence on the results. Due to homogeneous deformation and homogeneous thermal boundary conditions the distribution of temperature in the sample is constant, which implies zero temperature gradient.

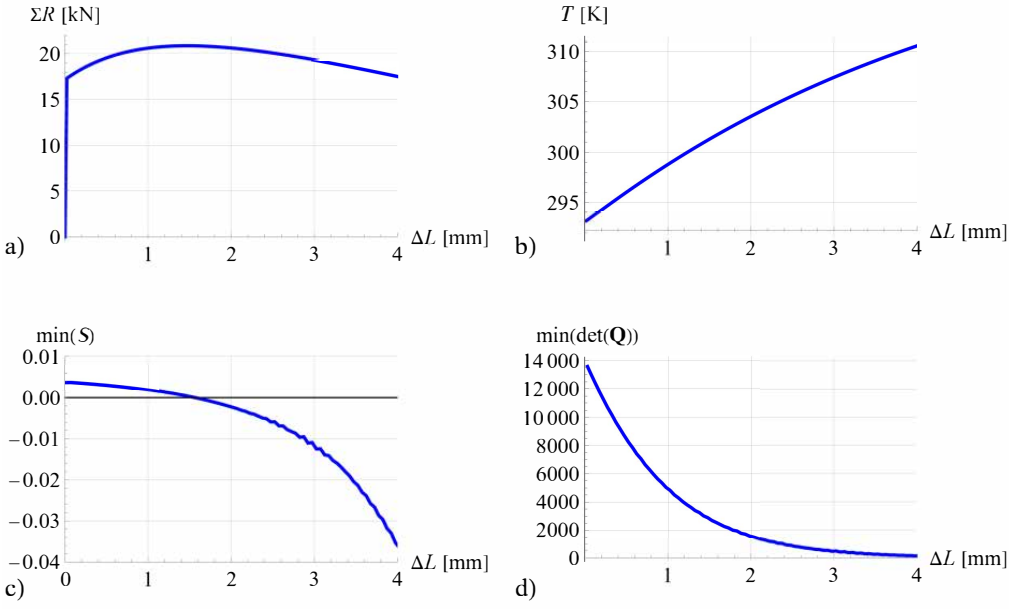

Fig. 2. Results for one finite element in simple shear – Test 1: a) sum of reactions in Z-direction, b) temperature in the sample, c) minimum value of term S in stability condition (Eq. (5.27)), d) minimum determinant of the acoustic tensor $\mathbf{Q}$ (Eqs. (5.9)–(5.10)).

The results obtained from the stability analysis are presented in Figs. 2c and 2d. In the former diagram the minimum value of term S (Eq. (5.27)) with respect to vector $\mathbf{N}$ is presented. The analysis is performed for the increment of angles α and β equal to $\pi/360$. The minor serrations observed on the curve result from angle discretization. The negative value of variable S appears for $\Delta L = 1.57$ mm, and when compared with Fig. 2a this occurs just after the onset of the decrease of the reaction sum for $\Delta L = 1.39$ mm. Simultaneously, the minimum value of the determinant of the acoustic tensor remains positive during the whole process. For the first step with a negative value of term S there

are two directions $\mathbf{N}$ for which the term S is less than zero. The first is obtained for $\alpha = 180$ deg and $\beta = 0.5$ deg, which corresponds almost to the X-axis, and the second for $\alpha = 0$ and $\beta = 81.5$ deg. The vector $\mathbf{N}$ refers to the undeformed configuration. In order to calculate its counterpart $\mathbf{n}$ in the current configuration, the formula $\mathbf{n} = \mathbf{F}^{-\mathrm{T}}\mathbf{N}/|\mathbf{F}^{-\mathrm{T}}\mathbf{N}|$ (valid for the material plane unit normal) is applied, which renders the critical direction $\mathbf{n}$ approximately consistent with the Z-direction for the second solution.

The results obtained from Test 2 are presented in Fig. 3. Although in the material models used for Test 1 and Test 2 the sources of softening are different

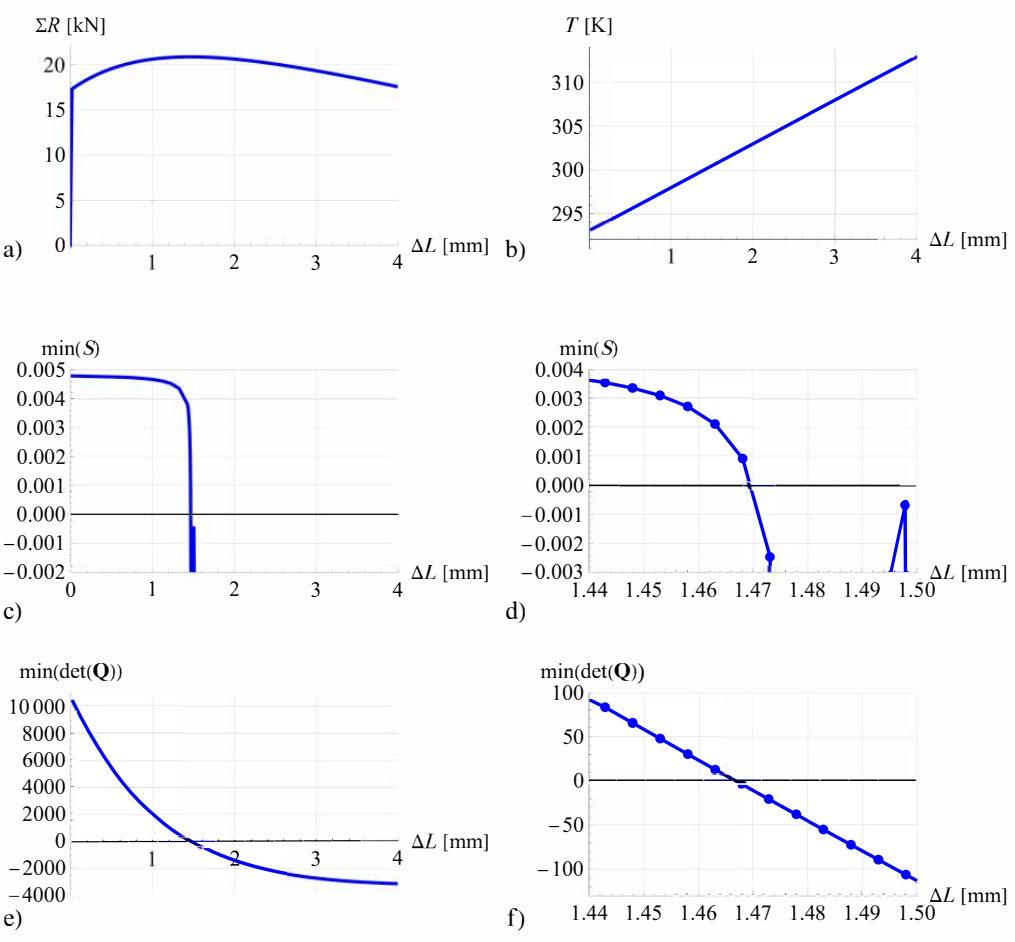

Fig. 3. Results for one finite element in simple shear – Test 2: a) sum of reactions in Z-direction, b) temperature in the sample, c) and d) minimum value of term S in stability condition (Eq. (5.27)), e) and f) minimum determinant of the acoustic tensor $\mathbf{Q}$ (Eqs. (5.9)–(5.10)). Diagrams c) and d) as well as e) and f) are for different ranges of axes. Dots in subfigures d) and f) mark time steps.

(in the first thermal, in the second material) the reactions are very similar, cf. the diagrams in Figs. 2a and 3a, whereas the temperature curves differ qualitatively and quantitatively, see the diagrams in Figs. 2b and 3b. The model with material softening exhibits a larger increase in temperature which grows almost linearly with loading. The main difference is observed for the stability analysis. The diagrams in Figs. 3c, 3d, 3e and 3f present the minimum values of S and $\det(\mathbf{Q})$ from the onset of plasticity until the enforced displacement equals $\Delta L = 4$ mm. Note that at the beginning of the plastic process the value of $\min(S)$ decreases with deformation but significantly slower than for Test 1, see the diagram in Fig. 2c. The drop in the value of $\min(S)$ observed for ΔL exceeding 1.4 occurs simultaneously with the appearance of negative values of the determinant of the acoustic tensor, which is confirmed by the analysis of this part of the process shown in the diagrams in Figs. 3d and 3f. It is mentioned that the jump of the value of $\min(S)$ for $\Delta L = 1.498$ mm, visible in Fig. 3c and clearly in Fig. 3d, is a result of too coarse angle discretization.

When comparing the results for Test 1 and Test 2 it can be seen that the thermal softening causes the loss of stability as indicated by the term S although the determinant of the acoustic tensor remains positive. The loss of stability appears simultaneously with the negative slope in the reaction diagram. For material softening, which results in similar reactions, stability is also lost when the reactions start to decrease, and the determinant of the acoustic tensor and stability indicator S becomes negative at the same time.

It is worth mentioning that the simple shear test does not involve all phenomena that can be reproduced by the presented thermo-elastoplastic model. In this test the thermo-elastic coupling does not result in a temperature change (the volume of the sample is constant during deformation). Moreover, due to the homogeneous distribution of temperature in the sample, the temperature gradient is zero and this implies the zero conductivity term $K\mathrm{Div}(\mathrm{Grad}(T))$ in the balance of energy (3.19). For this reason subsequent simulations are performed for a plate with an imperfection, subjected to tension.

7.2. Plate with imperfection

To investigate the stability condition for a complex stress state, simulations of a plate in tension are performed. The plate shown in Fig. 4 has the dimensions 20 mm, 10 mm and 0.25 mm, and due to symmetry only one fourth of the plate is implemented, marked in Fig. 4, in grey colour. The adopted discretization is shown in Fig. 5. At the central point of the original plate an imperfection is applied in the form of thickness reduction. The perturbed thickness there equals 0.225 mm. The imperfection is achieved by lowering the central node lying on the upper surface of the specimen. The plate is elongated in the X-direction

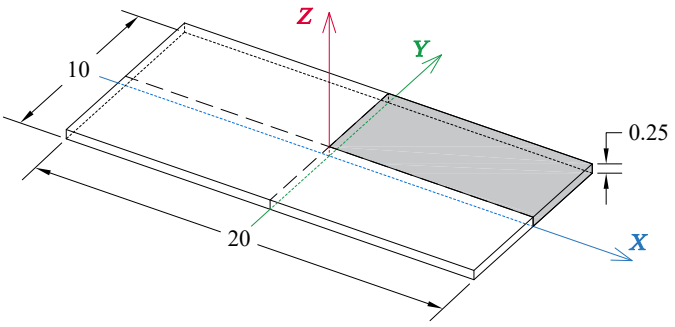

Fig. 4. Geometry of plate with imperfection, dimensions are in mm.

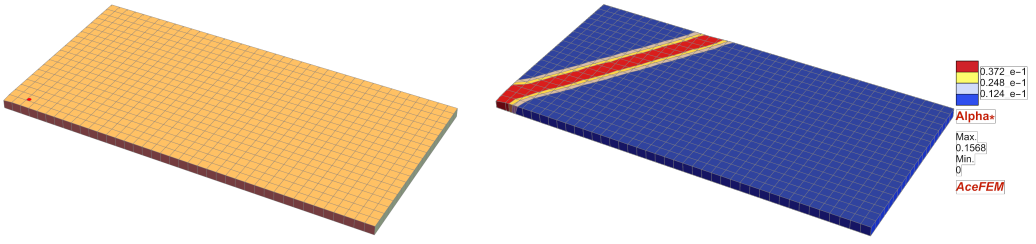

Fig. 5. Discretization of plate with imperfection (one-fourth of the specimen) with red dot denoting location of Gauss point selected for stability analysis (left). Contour plot of hardening variable α and deformed mesh at loading level $\Delta L = 0.06$ mm (right).

by enforced displacement applied with the rate 2 mm/s. Moreover, displacements in the Y-direction are unconstrained. Similarly to the simulations in Section 7.1, AceFEM built-in adaptive time stepping is used with the following parameters: the first time step is 10^{-3} s and, thereafter, the minimum and maximum time increments are 10^{-4} s and $5 \cdot 10^{-4}$ s, respectively.

Insulation is assumed for the whole plate boundary. The analysis of stability is performed at a selected point near the imperfection with coordinates $(0.5528, 0.3028, 0.1971)$ mm, marked by a red dot in Fig. 5.

The simulations are performed for three cases:

- isothermal model with linear material softening $H = -2.07$ GPa, the initial and final yield thresholds equal $\sigma_{y0} = \sigma_{y\infty} = 0.45$ GPa in Eq. (6.16), i.e., exponential hardening is not active,
- conductive thermo-elastoplastic material model with linear material softening $H = -2.07$ GPa and the initial and final yield thresholds equal $\sigma_{y0} = \sigma_{y\infty} = 0.45$ GPa in Eq. (6.16) and with inactive thermal softening $H_T = 0$ in Eq. (6.21),

- conductive thermo-elastoplastic material model with thermal softening $H_T = 0.18$ K^{-1} in Eq. (6.21) and initial and final yield thresholds $\sigma_{y0} = \sigma_{y\infty} = 0.35$ GPa in Eq. (6.16) and with inactive material softening $H = 0$ in Eq. (6.21).

The sets of plasticity parameters for the analysed cases are shown in Tables 4–6.

Table 4. Plasticity parameters for isothermal case.

Property	Symbol	Value	Unit
Initial yield threshold	σ_{y0}	0.45	GPa
Final yield threshold	$\sigma_{y\infty}$	0.45	GPa
Saturation constant	δ	16.93	–
Hardening modulus	H	−2.07	GPa

Table 5. Plasticity parameters for conductive case with linear material softening.

Property	Symbol	Value	Unit
Initial yield threshold	σ_{y0}	0.45	GPa
Final yield threshold	$\sigma_{y\infty}$	0.45	GPa
Saturation constant	δ	16.93	–
Hardening modulus	H	−2.07	GPa
Thermal softening modulus	H_T	0	K^{-1}

Table 6. Plasticity parameters for conductive case with thermal softening.

Property	Symbol	Value	Unit
Initial yield threshold	σ_{y0}	0.35	GPa
Final yield threshold	$\sigma_{y\infty}$	0.35	GPa
Saturation constant	δ	16.93	–
Hardening modulus	H	0	GPa
Thermal softening modulus	H_T	0.18	K^{-1}

The results obtained in the simulations are shown in Figs. 5–7. The deformed mesh with the distribution of hardening variable α obtained for the thermo-elastoplastic model with material softening for $\Delta L = 0.06$ mm is shown in Fig. 5. The hardening variable distributions for the remaining models are almost the same as the one shown in Fig. 5. Strain localization has a form of a shear band with origin at the imperfection. The selected point for stability analysis lies at the edge of the localization zone.

In Fig. 6 (left) it can be observed that the reaction diagram for the isothermal model (green line) is very close to its thermo-elastoplastic counterpart (blue line).

The slight difference is visible only in the elastic regime due to thermo-elastic coupling. The model with thermal softening exhibits a slightly different shape of the reaction curve for plasticity. The temperature evolution at the selected Gauss point, see Fig. 6 (right), is also similar for the two analysed models, although the model with thermal softening shows a nonlinear increase of temperature, smaller at the end of the elongation process.

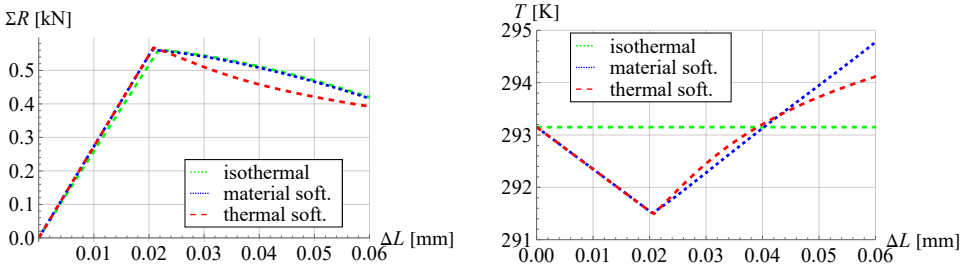

Fig. 6. Sum of reactions for plate in tension and evolution of temperature at selected Gauss point.

The analysis of stability at the selected Gauss point is performed only for the plastic steps. The left diagram of Fig. 7 shows the minimum values of the acoustic tensor for the three analysed models. The diagram obtained for the isothermal model with material softening (green line) is very close to its thermo-elastoplastic counterpart (blue line). Both of them become negative almost at the same time. The minimum determinant of the acoustic tensor for the model with thermal softening also decreases but remains positive until the end of the considered process. The analysis of the minimum value of the term S for the thermo-elastoplastic models is presented in the right diagram of Fig. 7. For the isothermal case (the green diagram), the term S is constant and independent of the direction $\mathbf{N}$. Its value is $S = \rho_0 c = 0.00345$. It cannot be treated as an indicator of stability in the isothermal case, for which this role is played by the determinant of the

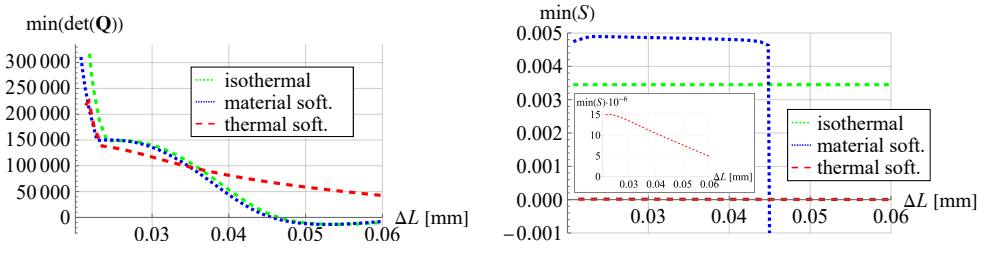

Fig. 7. Minimum determinant of acoustic tensor $\mathbf{Q}$ in Eqs. (5.9)–(5.10) (on the left) and minimum value of term S in stability condition in Eq. (5.27) (on the right) vs enforced displacement, both diagrams for selected Gauss point.

acoustic tensor. For the model with the material softening the term S is positive up to $\Delta L = 0.045$ mm and then abruptly decreases, and remains negative for the rest of the process. The determinant of the acoustic tensor for this model becomes negative exactly at the same load step. For the model with thermal softening the (absolute) value of the term S is much smaller than for the model with material softening. The magnified diagram of $\min(S)$ in Fig. 7 shows that its value decreased with the deformation and it remains positive in the analysed process. It can be concluded that in this case the enhancement of the isothermal model reproducing material softening with thermo-mechanical coupling does not improve the stability at the selected point. The loss of positive-definiteness of the acoustic tensor triggers a negative value of stability indicator S. The regularizing effect of the thermo-mechanical coupling, i.e., preserving the term S positive, is significant when softening has its origin in the reduction of the yield strength due to an increase in temperature.

8. Final remarks

The research presented in this paper deals with the stability of thermo-elastoplastic material models undergoing large strains. Based on the possibly general and thermodynamically consistent material description, the stability analysis has been performed using a perturbative approach. Special attention has been paid to the quasi-static conductive case, for which a specific stability condition has been formulated. It is shown in the paper that the derived condition can be analysed numerically to check whether additional regularization of the material model is needed.

For the purpose of this study a finite element algorithm for the presented model has been developed and tested with two examples. The application of the symbolic-numerical toolbox AceGen/FEM for computer simulations allowed for the implementation of the highly non-linear coupled problem.

Computer simulations performed for one finite element subjected to simple shear have shown that, in the case of thermal softening, the acoustic tensor possesses positive determinant while the stability term S becomes negative at the same moment when reactions start to decrease. In turn, the numerical analysis of shearing for material softening has revealed that the derived stability condition for thermo-elastoplasticity is violated at the same time when the determinant of the acoustic tensor becomes negative. The verification of the derived stability condition is thus necessary to indicate the stability loss in the case where the source of softening is related to thermal effects. Although the overall response of the material can be similar for various types of softening, the analysis of stability reveals significant differences. In the presented test of the plate in tension the regularizing effect of heat conduction is visible when softening is trig-

gered by thermal effects. The thermo-mechanical coupling does not significantly influence the results obtained for the material model accounting only for material softening.

The numerical analysis of stability condition involves finding the minimum of a term dependent on the direction vector. The method which is applied in the paper is based on the discretization of the space of direction vectors. It should be mentioned that the approach is computationally expensive and has limited accuracy. Further investigations are planned to address this problem and to propose more efficient methods.

Appendix A

This appendix summarizes notation for vector and tensor products used in this paper. Let us assume that, for instance, α represents a scalar, boldface lowercase letters, e.g., $\mathbf{a}$, denote vectors with coefficients a_i, boldface uppercase letters, e.g., $\mathbf{A}$, denote second order tensors with coefficients A_{ij}, calligraphic uppercase letters, e.g., $\mathcal{A}$, denote third order tensors with coefficients A_{ijk} and blackboard bold uppercase letters, e.g., $\mathbb{A}$, denote fourth order tensors with coefficients A_{ijkl}. In all cases we assume that components are referred to an orthonormal basis. Table 7 summarizes notation used for related products of tensors and highlights absolute as well as index notation. Moreover, derivatives of (and with respect to) vectors and tensors are represented in index notation as, e.g.,

$$\left[\frac{\partial \mathbf{a}}{\partial \mathbf{b}}\right]_{ij} = \frac{\partial a_i}{\partial b_j} \quad \text{and} \quad \left[\frac{\partial \mathbf{C}}{\partial \mathbf{D}}\right]_{ijkl} = \frac{\partial C_{ij}}{\partial D_{kl}}. \tag{8.1}$$

Table 7. Overview on notation used for tensor operations.

Abs. notation	Index notation	Abs. notation	Index notation
$\mathbf{a}\cdot\mathbf{b}=\alpha$	$\alpha = a_i b_i$	$\mathbf{B}\cdot\mathbf{a}=\mathbf{c}$	$c_i = B_{ij}a_j$
$\mathbf{a}\cdot\mathbf{B}=\mathbf{c}$	$c_i = a_j B_{ji}$	$\mathbf{A}:\mathbf{B}=\alpha$	$\alpha = A_{ij}B_{ij}$
$\mathbf{A}\cdot\mathbf{B}=\mathbf{C}$	$C_{ij} = A_{ik}B_{kj}$	$\mathcal{B}\cdot\mathbf{a}=\mathbf{C}$	$C_{ij} = B_{ijk}a_k$
$\mathbf{a}\cdot\mathcal{B}=\mathbf{C}$	$C_{ij} = a_k B_{kij}$	$\mathcal{B}:\mathbf{C}=\mathbf{a}$	$a_i = B_{ijk}C_{jk}$
$\mathbf{C}:\mathcal{B}=\mathbf{a}$	$a_i = C_{jk}B_{jki}$	$\mathcal{B}:\mathcal{C}=\mathbf{A}$	$A_{ij} = B_{ikl}C_{klj}$
$\mathcal{A}\cdot\mathcal{B}=\mathbb{C}$	$C_{ijkl} = A_{ijm}B_{mkl}$	$\mathbf{A}:\mathbb{C}=\mathbf{B}$	$B_{ij} = A_{kl}C_{klij}$
$\mathbb{B}\cdot\mathbf{a}=\mathcal{C}$	$C_{ijk} = B_{ijkl}a_l$	$\mathbb{C}:\mathbf{B}=\mathbf{A}$	$A_{ij} = C_{ijkl}B_{kl}$
$\mathbb{C}\vdots\mathcal{B}=\mathbf{a}$	$a_i = C_{ijkl}B_{jkl}$	$\mathbb{A}:\mathbb{B}=\mathbb{C}$	$C_{ijkl} = A_{ijmn}B_{mnkl}$
$\mathbf{a}\otimes\mathbf{b}=\mathbf{C}$	$C_{ij} = a_i b_j$	$\mathbf{B}\otimes\mathbf{a}=\mathcal{C}$	$C_{ijk} = B_{ij}a_k$
$\mathbf{A}\otimes\mathbf{B}=\mathbb{C}$	$C_{ijkl} = A_{ij}B_{kl}$	$\mathcal{B}=\mathcal{A}^T$	$B_{ijk} = A_{kij}$

Appendix B

The derivatives of perturbations presented in Eqs. (5.5) and (5.6) are summarised in Table 8 using absolute and index notation.

Table 8. Overview on derivatives in space and time of displacement and temperature perturbations.

Absolute notation	Index notation
$\dfrac{\partial \mathbf{u}^{pert}}{\partial \mathbf{X}} = ik\exp(ik\mathbf{N}\cdot\mathbf{X}-i\omega t)\hat{\mathbf{u}}\otimes\mathbf{N}$	$\dfrac{\partial u_k^{pert}}{\partial X_J} = ik\exp(ikN_M X_M-i\omega t)\hat{u}_k N_J$
$\dfrac{\partial^2 \mathbf{u}^{pert}}{\partial \mathbf{X}\partial \mathbf{X}} = -k^2\exp(ik\mathbf{N}\cdot\mathbf{X}-i\omega t)\hat{\mathbf{u}}\otimes\mathbf{N}\otimes\mathbf{N}$	$\dfrac{\partial^2 u_k^{pert}}{\partial X_J\partial X_L} = -k^2\exp(ikN_M X_M-i\omega t)\hat{u}_k N_J N_L$
$\dot{\mathbf{u}}^{pert} = -i\omega\exp(ik\mathbf{N}\cdot\mathbf{X}-i\omega t)\hat{\mathbf{u}}$	$\dot{u}_k^{pert} = -i\omega\exp(ikN_M X_M-i\omega t)\hat{u}_k$
$\ddot{\mathbf{u}}^{pert} = -\omega^2\exp(ik\mathbf{N}\cdot\mathbf{X}-i\omega t)\hat{\mathbf{u}}$	$\ddot{u}_k^{pert} = -\omega^2\exp(ikN_M X_M-i\omega t)\hat{u}_k$
$\dfrac{\partial \dot{\mathbf{u}}^{pert}}{\partial \mathbf{X}} = k\omega\exp(ik\mathbf{N}\cdot\mathbf{X}-i\omega t)\hat{\mathbf{u}}\otimes\mathbf{N}$	$\dfrac{\partial \dot{u}_k^{pert}}{\partial X_J} = k\omega\exp(ikN_M X_M-i\omega t)\hat{u}_k N_J$
$\dfrac{\partial T^{pert}}{\partial \mathbf{X}} = ik\exp(ik\mathbf{N}\cdot\mathbf{X}-i\omega t)\hat{T}\,\mathbf{N}$	$\dfrac{\partial T^{pert}}{\partial X_J} = ik\exp(ikN_M X_M-i\omega t)\hat{T}N_J$
$\mathrm{Div}(\mathrm{Grad}(T^{pert})) = -k^2\hat{T}\exp(ik\mathbf{N}\cdot\mathbf{X}-i\omega t)$	$\mathrm{Div}(\mathrm{Grad}(T^{pert})) = -k^2\hat{T}\exp(ikN_M X_M-i\omega t)$
$\dot{T}^{pert} = -i\omega\exp(ik\mathbf{N}\cdot\mathbf{X}-i\omega t)\hat{T}$	$\dot{T}^{pert} = -i\omega\exp(ikN_M X_M-i\omega t)\hat{T}$

Acknowledgements

The work is supported within the Weave-UNISONO program by the German Research Foundation (DFG grant 527828607) and by the National Science Centre, Poland (NCN grant 2023/05/Y/ST8/00006).

References

1. R. Hill, *A general theory of uniqueness and stability in elastic-plastic solids*, Journal of the Mechanics and Physics of Solids, **6**, 236–249, 1958.
2. Y. Thomas, *Plastic Flow and Fracture of Solids*, Academic Press, New York, 1961.
3. J.R. Rice, *The localization of plastic deformation*, [in:] W.T. Koiter [ed.], Proceedings of the 14th International Congress of Theoretical and Applied Mechanics, pp. 207–220, North-Holland Publishing Company, Amsterdam, 1976.
4. Z.P. Bažant, G. Pijaudier-Cabot, *Nonlocal continuum damage, localization instability and convergence*, ASME Journal of Applied Mechanics, **55**, 287–293, 1988.
5. J.C. Simo, *Strain softening and dissipation: A unification of approaches*, [in:] J. Mazars, Z.P. Bažant [eds.], Cracking and Damage: Strain Localization and Size Effect, pp. 440–461, Elsevier Applied Science, London–New York, 1989.

6. A. Needleman, *Continuum mechanics studies of plastic instabilities*, Revue de Physique Appliquée, **23**, 585–593, 1988.
7. A. Needleman, V. Tvergaard, *Analyses of plastic flow localization in metals*, ASME Applied Mechanics Reviews, **45**, 3–17, 1992.
8. H.M. Zbib, E.C. Aifantis, *On the localization and postlocalization behavior of plastic deformation (Parts I, II, III)*, Res Mechanica, **23**, 261–305, 1988.
9. N.S. Ottosen, K. Runesson, *Properties of discontinuous bifurcation solutions in elasto-plasticity*, International Journal of Solids and Structures, **27**, 4, 401–421, 1991.
10. V. Tvergaard, *Studies of elastic-plastic instabilities*, ASME Journal of Applied Mechanics, **66**, 3–9, 1999.
11. G. Maier, T. Hueckel, *Nonassociated and coupled flow rules of elastoplasticity for rock-like materials*, International Journal of Rock Mechanics and Mining Sciences and Geomechanics Abstracts, **16**, 2, 77–92, 1979.
12. D. Bigoni, H. Petryk, *A note on divergence and flutter instabilities in elastic-plastic materials*, International Journal of Solids and Structures, **39**, 911–926, 2002.
13. A. Benallal, C. Comi, *Material instabilities in inelastic saturated porous media under dynamic loadings*, International Journal of Solids and Structures, **39**, 3693–3716, 2002.
14. L.J. Sluys, *Wave propagation, localization and dispersion in softening solids*, Ph.D. dissertation, Delft University of Technology, Delft, 1992.
15. R. de Borst, L.J. Sluys, H.-B. Mühlhaus, J. Pamin, *Fundamental issues in finite element analyses of localization of deformation*, Engineering with Computers, **10**, 99–121, 1993.
16. P.B. Béda, *Dynamical systems, rate and gradient effects in material instability*, International Journal of Mechanical Sciences, **42**, 2101–2114, 2000.
17. T. Liebe, P. Steinmann, *Theory and numerics of a thermodynamically consistent framework for geometrically linear gradient plasticity*, International Journal for Numerical Methods in Engineering, **51**, 1437–1467, 2001.
18. S. Forest, E. Lorentz, *Localization phenomena and regularization methods*, [in:] J. Besson [ed.], Local approach to fracture, pp. 311–370, Les Presses de l'École des Mines, Paris, 2004.
19. H. Petryk, *Plastic instability: Criteria and computational approaches*, Archives of Computational Methods in Engineering, **4**, 2, 111–151, 1997.
20. P. Steinmann, R. Larsson, K. Runesson, *On the localization properties of multiplicative hyperelasto-plastic continua with strong discontinuities*, International Journal of Solids and Structures, **34**, 8, 969–990, 1997.
21. R. Khen, T. Désoyer, A. Dragon, *Objective localization criterion and behaviour for finite deformation plasticity – a Lagrangian formulation*, Archive of Applied Mechanics, **68**, 85–102, 1998.
22. H. Petryk, *Thermodynamic conditions for stability in materials with rate-independent dissipation*, Philosophical Transactions of the Royal Society A, **363**, 2479–2515, 2005.
23. I. Vardoulakis, J. Sulem, *Bifurcation Analysis in Geomechanics*, Blackie Academic & Professional, London, 1995.

24. P. Perzyna [ed.], *Localization and Fracture Phenomena in Inelastic Solids*, CISM Course Lecture Notes No. 386, Springer-Verlag, Wien, 1998.

25. Q.S. Nguyen, *Stability and Nonlinear Solid Mechanics*, John Wiley & Sons, Chichester, 2000.

26. H. Petryk [ed.], *Material Instabilities in Elastic and Plastic Solids*, CISM Course Lecture Notes No. 414, Springer-Verlag, Wien, 2000.

27. D. Bigoni, *Nonlinear Solid Mechanics: Bifurcation Theory and Material Instability*, Cambridge University Press, Cambridge, 2012.

28. J. Utzinger, A. Menzel, P. Steinmann, A. Benallal, *Aspects of bifurcation in an isotropic elastic continuum with orthotropic inelastic interface*, European Journal of Mechanics – A/Solids, **27**, 4, 532–547, 2008.

29. J. LeMonds, A. Needleman, *Finite element analyses of shear localization in rate and temperature dependent solids*, Mechanics of Materials, **5**, 339–361, 1986.

30. Y. Tomita, *Simulations of plastic instabilities in solid mechanics*, Applied Mechanics Reviews **47**, 6, 171–205, 1994.

31. A. Benallal, D. Bigoni, *Effects of temperature and thermo-mechanical couplings on material instabilities and strain localization of inelastic materials*, Journal of the Mechanics and Physics of Solids, **52**, 725–753, 2004.

32. R.C. Batra, C.H. Kim, *Effect of thermal conductivity on the initiation, growth and bandwidth of adiabatic shear bands*, International Journal of Engineering Science, **29**, 8, 949–960, 1991.

33. H.T. Zhu, H.M. Zbib, E.C. Aifantis, *On the role of strain gradients in adiabatic shear banding*, Acta Mechanica, **111**, 111–124, 1995.

34. B. Dodd, Y. Bai, *Introduction to Adiabatic Shear Localization*, Imperial College Press, London, revised ed., 2015.

35. R. Abeyaratne, J.K. Knowles, *On the stability of thermoelastic materials*, Journal of Elasticity, **53**, 199–213, 1999.

36. J. Dunwoody, R.W. Ogden, *On the thermodynamic stability of elastic heat-conducting solids subject to a deformation-temperature constraint*, Mathematics and Mechanics of Solids, **7**, 285–306, 2002.

37. B.D. Reddy, *The propagation and growth of acceleration waves in constrained thermoelastic materials*, Journal of Elasticity, **14**, 387–402, 1984.

38. P. Perzyna, *Adiabatic shear-band localization fracture of solids in dynamic loading processes*, Journal de Physique IV Proceedings, **4**, C8, 411–446, 1994.

39. M.K. Duszek, P. Perzyna, E. Stein, *Adiabatic shear band localization in elastic-plastic damaged solids*, International Journal of Plasticity, **8**, 4, 361–384, 1992.

40. T. Łodygowski, *Theoretical and Numerical Aspects of Plastic Strain Localization*, Monograph 312, Poznań University of Technology, Poznań, 1996.

41. P.A. Wriggers, C. Miehe, M. Kleiber, J.C. Simo, *On the coupled thermomechnical treatment of necking problems via finite element methods*, International Journal for Numerical Methods in Engineering, **33**, 869–883, 1992.

42. T. Liebe, P. Steinmann, A. Benallal, *Theoretical and computational aspects of a thermodynamically consistent framework for geometrically linear gradient damage*, Computer Methods in Applied Mechanics and Engineering, **190**, 6555–6576, 2001.

43. R.H.J. Peerlings, R. de Borst, W.A.M. Brekelmans, J.H.P. de Vree, *Gradient-enhanced damage for quasi-brittle materials*, International Journal for Numerical Methods in Engineering, **39**, 3391–3403, 1996.

44. B. Wcisło, J. Pamin, K. Kowalczyk-Gajewska, *Gradient-enhanced damage model for large deformations of elastic-plastic materials*, Archives of Mechanics, **65**, 5, 407–428, 2013.

45. B. Wcisło, J. Pamin, *Local and non-local thermomechanical modeling of elastic-plastic materials undergoing large strains*, International Journal for Numerical Methods in Engineering, **109**, 1, 102–124, 2017.

46. R. de Borst, H.-B. Mühlhaus, *Gradient-dependent plasticity: Formulation and algorithmic aspects*, International Journal for Numerical Methods in Engineering, **35**, 521–539, 1992.

47. J. Korelc, P. Wriggers, *Automation of Finite Element Methods*, Springer, 2016.

48. M. Ristinmaa, *Thermodynamic formulation of plastic work hardening materials*, ASCE Journal of Engineering Mechanics, **125**, 152–155, 1999.

49. J. Bonet, R.D. Wood, *Nonlinear Continuum Mechanics for Finite Element Analysis*, 2nd ed., Cambridge University Press, Cambridge, 2008.

50. J.C. Simo, *Numerical analysis and simulation of plasticity*, [in:] P.G. Ciarlet, J.L. Lions [eds.], Handbook of Numerical Analysis, vol. IV, pp. 183–499, Elsevier Science B.V., Boca Raton, 1998.

51. P. Oppermann, R. Denzer, A. Menzel, *A thermo-viscoplasticity model for metals over wide temperature ranges- application to case hardening steel*, Computational Mechanics, **69**, 541–563, 2022.

52. B. Wcisło, J. Pamin, L. Rose, A. Menzel, *On spatial vs. referential isotropic Fourier's law in finite deformation thermomechanics*, Engineering Transactions, **71**, 1, 111–140, 2023.

53. S. Kaliski, *Technical Mechanics, Vol. 3: Vibrations and Waves* [in Polish], PWN, Warszawa, 1986.

54. M. Taboga, *Lectures on Linear Algebra*, Independently published, 1st ed., 2021, https://www.statlect.com/matrix-algebra/.

55. M. Ristinmaa, M. Wallin, N.S. Ottosen, *Thermodynamic format and heat generation of isotropic hardening plasticity*, Acta Mechanica, **194**, 103–121, 2007.

56. J. Korelc, *Automation of primal and sensitivity analysis of transient coupled problems*, Computational Mechanics, **44**, 631–649, 2009.

57. E.A. de Souza Neto, D. Perić, M. Dutko, D.R.J. Owen, *Design of simple low order finite elements for large strain analysis of nearly incompressible solids*, International Journal of Solids and Structures, **33**, 20, 3277–3296, 1996.

58. J. Korelc, S. Stupkiewicz, *Closed-form matrix exponential and its application in finite-strain plasticity*, International Journal for Numerical Methods in Engineering, **13**, 98, 960–987, 2014.

59. B. Wcisło, J. Pamin, K. Kowalczyk-Gajewska, A. Menzel, *Numerical analysis of ellipticity condition for large strain plasticity*, [in:] AIP Conference Proceedings, vol. 1922, p. 140008, 2018.

60. J. Korelc, *AceGen and AceFEM User Manual*, University of Ljubljana, 2011, avaliable from: http://symech.fgg.uni-lj.si.

Received December 31, 2024; revised version September 26, 2025.
Published online October 23, 2025.